Physics – Uspekhi **45** (5) 527 – 552 (2002)

REVIEWS OF TOPICAL PROBLEMS PACS numbers: **66.70.+f**, **72.10.–d**, 72.15.Eb, 72.20.Pa

Kinetic coefficients in isotopically disordered crystals

A P Zhernov, A V Inyushkin

DOI: 10.1070/PU2002v045n05ABEH001084

Contents

Abstract. Peculiarities of the behavior of kinetic coefficients, like thermal conductivity, electric conductivity, and thermoelectric power, in isotopically disordered materials are reviewed in detail. New experimental and theoretical results on the isotope effects in the thermal conductivity of diamond, Ge, and Si semiconductors are presented. The suppression effect of phonon-drag thermopower in the isotopically disordered Ge crystals is discussed. The influence of dynamic and static crystal lattice deformations on the electric conductivity of metals as well as on the ordinary phonon spectrum deformations is considered.

1. Introduction

Generally speaking, the problem of the effects of isotopic disorder on the kinetic coefficients of crystals has not been studied in too much detail. For example, until quite recently one would find in the scientific literature just a few papers containing experimental findings concerned with the investigations of peculiarities of the behavior of thermal conductivity and thermoelectric power of semiconductors or of the electric resistance of metals. This is primarily due to the considerable difficulties in the preparation of chemically pure and practically perfect single crystals with the 'hand-made' isotopic composition, including the case of highly enriched systems. Naturally, the practical absence of experimental data hampered theoretical developments based essentially on the classical works by I Ya Pomeranchuk.

In 1990s, through the joint effort of specialists from Russia, USA, Germany and Japan, bulk single crystals of diamond, germanium and silicon with different isotopic compositions were grown. Specimens of these and other semiconductors were used for experimental and theoretical studies of the effects of isotopic composition on the phonon and electronic spectra, on structural properties, as well as thermal conductivity and thermoelectric power. Notice that the studies of thermal conductivity were also concerned with the issues related to the high anisotropy of the germanium and silicon phonon spectra, the interference between different mechanisms of phonon scattering, the clarification of the role of acoustical and optical modes. This review is mainly devoted to the analysis of results on the kinetics of these phenomena.

We also included in this review the material on the electric resistivity ρ of isotopically disordered metals. In the first place we discuss the experimental data on cadmium and lithium, obtained at the Russian Research Centre "Kurchatov Institute" in the 1970s and 80s. Observe that lithium metal has been theoretically studied rather well and has a relatively simple structure of Fermi surface (FS). This allowed separation of the contributions into ρ coming from the isotopic deformation of the phonon spectrum (the first-order effect in ΔM), and from the effect of 'masking' of the fine structure of the nonequilibrium electron distribution function ('hot spots' on FS) through the presence of chemical impurities. In addition, in this review we discuss the topic of influence of static disorder, caused by the dynamic isotopic disordering, on the residual resistivity of practically chemically pure metals. Apparently, a similar effect was observed by Zernov and Sharvin in tin single crystals.

A P Zhernov Institute of Superconductivity and Solid State Physics, Russian Research Centre 'Kurchatov Institute'
A V Inyushkin Institute of Molecular Physics, Russian Research Centre 'Kurchatov Institute', pl. Kurchatova 1, 123182 Moscow, Russian Federation
Tel. (7-095) 196 74 28. Fax (7-095) 194 19 94
E-mail: inyushkin@imp.kiae.ru

Received 19 June 2001
Uspekhi Fizicheskikh Nauk **172** (5) 573 – 599 (2002)
Translated by A S Dobroslavskiĭ; edited by A Radzig

2. Isotopic disorder effects in the phonon thermal conductivity of nonmetals

Crystals constituted by a mixture of isotopes exhibit dynamic disorder because of the different masses of the same atoms at different lattice sites — the amplitude and the phase of oscillations of the 'impurity' isotope are not similar to those of the isotopes that form the crystal matrix. This dynamic disorder breaks the translational symmetry of the lattice, and so phonons are no longer the pure eigenstates of the crystal harmonic Hamiltonian. The influence of impurity isotopes on the phonons can be described in terms of the temperature-independent isotope scattering of phonons. It turns out that for chemically pure and structurally perfect dielectric crystals this isotope scattering may play the definitive role in thermal conductivity at low temperatures. It is interesting that the concrete theoretical estimates [1, 2] of such a role of isotope scattering were made before the first experiment of Geballe and Hull [3] that discovered the isotope effect in germanium thermal conductivity. Dynamic disordering in crystals also leads to static disorder — fluctuating fields of static lattice deformations. Scattering of phonons by such lattice distortions around the isotopic impurity in conventional nonquantum crystals is much less than the scattering caused by the dynamic disorder.

In practice, the analysis of experimental data usually relies on the simplified phenomenological approaches based on the relaxation time approximation and assuming independence of the different processes of nonequilibrium phonon scattering [4]. For example, the low-temperature thermal conductivity of not highly pure crystals is often very adequately described with the so-called Debye model (see, for example, Ref. [5]) which only considers the resistive phonon scattering processes — that is, processes that do not conserve the momentum in the phonon subsystem: scattering of phonons by the boundaries of the specimen, by lattice defects and impurities (including isotopes), and the inelastic anharmonic transitions accompanying umklapp processes (U-processes). In the case of near-perfect (structurally) single crystals with a high degree of isotope enrichment, which are the object of our attention in this review, the stationary distribution of nonequilibrium phonons may be to a large extent determined, in addition to the resistive processes, also by the nonresistive anharmonic nonumklapp processes (N-processes). The role of N-processes becomes especially important at low temperatures, when the U-processes freeze out, and the thermal conductivity passes through a maximum. Several theoretical models taking into account the special role of normal processes in heat conduction were proposed with this aim in view (see, for example, a brief review in Berman's paper [5]). The most successful proved to be the Callaway theory [6] which makes it relatively easy to evaluate the importance of different phonon scattering processes.

The thermal conductivity tensor in its most general form is represented by the Kubo formula which involves the pair correlation function constructed in terms of operators of phonon heat flux (see, for example, monograph [7]). Making use of the Kubo formula, the problem of heat conduction can be reduced in the first approximation to solving the equation of the kinetic type. In principle, it is possible then to take into account the corrections to the standard kinetic equation (see, for example, Ref. [8]). The most general method of solving the kinetic equation is the moments method [9]. It ought to be noted that the straightforward solution of the kinetic equation is associated with extremely cumbersome calculations because the scattering operator contains terms describing the anharmonic interaction of phonons. Sometimes the solution of the kinetic equation is sought by the iterative method [10 – 12]. Recently, with the advent of powerful supercomputers, numerical methods of molecular dynamics started to develop, based on the Kubo formalism [13 – 16]. Even with the modern supercomputers, however, such calculations take a plenty of time.

In this section we start off with presenting the main results of the Callaway theory, and then discuss the experimental findings. The main attention is paid to the role of isotope scattering process, and to the role of anharmonism. Along with the single-mode approximation which does not distinguish between longitudinal and transverse phonons, we also use the two-mode model which allows one to take into account the high anisotropy of the phonon spectrum. In addition, we discuss the experiments for germanium and silicon, based on the results obtained by the straightforward solution of the kinetic equation. The harmonic and anharmonic interactions of phonons are described in this case with the contemporary phenomenological models. In particular, we use this approach when discussing the effects of optical phonons on the behavior of $\varkappa(T)$. In Appendix A we present the consistent procedure for the selection of symmetrized linearly independent moments for crystals displaying different symmetry.

2.1 The Callaway model: single-mode case

2.1.1 Basic relations. The analysis of experimental data on the lattice thermal conductivity is often based on the Callaway theory [6] which takes into account the various processes of phonon relaxation (see also Refs [4, 17]). The Callaway theory takes into consideration the nontrivial role of N-processes and gives a relatively simple formula for thermal conductivity that involves the relaxation rates for a number of processes. The formula of interest is derived under certain simplifying assumptions which generally restrict the applicability of the theory by the region of low temperatures. To be more precise, the phonon modes are described in the Debye approximation, and no distinction is made between longitudinal (l) and transverse (t) modes. At the same time, the relaxation rates of phonon modes are expressed as simple power functions of frequency and temperature. In particular, it was assumed that the relaxation rate due to isotopes is proportional to ω^4. The expressions for relaxation rates of N- and U-processes include parameters found by fitting the experimental dependences. One important advantage of the Callaway theory is that it yields correct results in the known limiting cases of strong normal processes and frequency-independent resistive processes.

According to the Callaway theory, thermal conductivity is given by a formula of the type

$$\varkappa(T) = \varkappa_1 + \varkappa_2 \,, \tag{2.1}$$

where

$$\varkappa_1 = GT^3\langle\tau_C\rangle, \tag{2.2a}$$

$$\varkappa_2 = \frac{GT^3\langle\tau_C/\tau_N\rangle^2}{\langle\tau_C/(\tau_N\tau_R)\rangle} \,, \tag{2.2b}$$

$$G = \frac{k_B^4}{2\pi^2\hbar^3 v_s} \,,$$

and v_s is the average velocity of sound. By τ_C^{-1}, τ_R^{-1} and τ_N^{-1} we denoted the combined relaxation rate of phonons, the total relaxation rate of resistive processes, and the rate of nonresistive normal anharmonic processes, so that

$$\tau_C^{-1} = \tau_R^{-1} + \tau_N^{-1} . \tag{2.3}$$

The symbol $\langle \ldots \rangle$ is interpreted as follows

$$\langle f \rangle = \int_0^{T_D/T} \frac{x^4 \exp x}{(\exp x - 1)^2} f(x)\, dx .$$

The first term $\varkappa_1$ in the Callaway formula (2.1) is standard (or regular), whereas the additional term $\varkappa_2$ describes the specific role of normal anharmonic processes.

In the situation when the resistive processes dominate ($\tau_N \gg \tau_R$), the principal term in expression (2.1) for thermal conductivity is the first one. Alternatively, in very pure crystals at low temperatures, when thermal conductivity reaches its highest value, the intensity of resistive processes is less than that of the N-processes. In such a situation, at $\tau_N \ll \tau_R$ and $\tau_C \to \tau_N$, the behavior of thermal conductivity is determined by the second term $\varkappa_2$, and the thermal resistance is given by

$$W = \frac{1}{\varkappa_2} = \frac{\langle \tau_R^{-1} \rangle}{G\, T^3 \langle 1 \rangle^2} = \sum_j W_j , \tag{2.4}$$

where $\tau_R^{-1} = \sum_j \tau_j^{-1}$.

From the last relation we see that in the case under consideration the thermal resistance W shows no explicit dependence on the normal processes. Furthermore, the contributions into W from different resistive processes add up. Observe that the quantity $\varkappa \propto \varkappa_2$ essentially depends on the degree of isotopic disorder in the lattice, which explains the strong suppression of thermal conductivity in the neighborhood of the maximum even at low concentrations of the 'impurity' isotopes (see specific examples below).

Let us look at the explicit expressions for the relaxation rates. First, for the boundary scattering in the regime of diffuse reflection of phonons from the specimen surface we have

$$\tau_b^{-1} = v_s (l_c^{-1} + l_s^{-1}) , \tag{2.5a}$$

where

$$v_s^{-1} = \frac{1}{3} \left[2 v_t^{-1} + v_l^{-1} \right] . \tag{2.5b}$$

Here, l_c is the Casimir length, and l_s is the specimen length (the direction of propagation of heat flux). For a specimen of rectangular cross section with the area S, the Casimir length is $l_c = 1.12\sqrt{S}$ (see, for example, Refs [18, 19]).

The scattering processes related to isotopic disorder are characterized by the relaxation rate τ_{iso}^{-1} which has the following form (see, for example, Ref. [4]):

$$\tau_{iso}^{-1} = \xi^2 \frac{\pi \Omega_0}{6} \omega^2 \rho(\omega) , \tag{2.6a}$$

where $\xi^2 = \sum_i c_i (\Delta M_i / M)^2$ is the parameter of isotopic disorder, Ω_0 is the volume per one atom, and $\rho(\omega)$ is the density of phonon states of all modes. In the single-mode Callaway model, the phonons are described in the Debye approximation. Since $\tau_{iso}^{-1} \sim \omega^2 \rho(\omega)$, in the Debye approximation, when $\rho(\omega) \sim \omega^2$, expression (2.6) rearranges to a well-known 'Rayleigh-type' formula [20]

$$\tau_{iso}^{-1} = \xi^2 \frac{\Omega_0}{4\pi v_s^3} \omega^4 . \tag{2.6b}$$

In crystals with strong lattice anharmonism and in quantum crystals, the scattering of phonons by lattice deformations near the isotopic impurity may be important (see a brief review in Ref. [21]). If the lattice irregularity due to the fields of near-impurity static displacements is taken into account, formula (2.6b) for the scattering rate holds, but the disorder parameter increases and assumes the following form [20, 22]

$$\tilde{\xi}^2 \approx \xi^2 + 2 \sum_i c_i \left(\frac{\Delta \varphi_i}{\varphi} - 6.4\gamma \frac{\Delta r_i}{r} \right)^2 . \tag{2.7}$$

Here, the parameters $\Delta\varphi_i/\varphi$ and $\Delta r_i/r$ describe the relative variations of the local force constants and the influence of the static atomic displacements, and γ is the Grüneisen constant. It is interesting that in the circumstances of strong anharmonism the rate of phonon isotope scattering depends on temperature and decreases with increasing temperature. The source of this temperature dependence is the second term in expression (2.7). In the classical limit we have $\tilde{\xi}^2 \to \xi^2$, i.e. this quantity is determined by the measure of disorder arising from the fluctuation of mass from one lattice site to another.

Now let us turn to the description of anharmonic processes for longitudinal and transverse phonon modes. The relaxation rates due to U-processes for the phonon modes are represented in the form

$$\tau_U^{(i)-1} = A_U^{(i)} \omega^2 T^m \exp\left(-\frac{B^{(i)}}{T} \right) , \quad i = t, l , \tag{2.8}$$

where $m = 1-3$. In the region of high temperatures we have $\tau_U^{(i)-1} \sim \omega^2 T$.

The situation with the relaxation rates attributed to the normal three-phonon processes is as follows. As is well known, there is the problem of relaxation of the long-wave longitudinal phonons. Namely, in the isotropic medium the laws of conservation of energy and momentum forbid processes that could involve three phonons belonging to the same branch. In this connection, the theory considers the processes of Herring [23] and Simons [24, 25]. In the case of Herring processes, the deviation of a real crystal symmetry from isotropic is taken into account explicitly, so that the degeneration of the acoustic transverse branches becomes possible. Depending on the crystal symmetry, the degeneracy locus may be a surface, a line, or simply points. The locus may extend to the band boundaries. In the neighborhood of the degeneracy points the conservation laws hold, and the interaction is possible between a low-frequency l-phonon and a t_1-phonon of one of the degenerate branches with the formation of a t_2-phonon of another degenerate branch (the t_1 branch lies above the t_2 branch). The smallness of the phase volume for similar almost-degenerate frequencies gives the corresponding relatively high powers of the frequency of a longitudinal phonon in the expressions for the inverse relaxation time.

In the case of Simons processes we are dealing with the interaction between a low-frequency longitudinal phonon and a thermal longitudinal phonon with the formation of a

phonon of the same polarization. As noted above, for isotropic medium such a process is not allowed. However, it can be realized if we take into account the finite lifetime of a thermal phonon.

As a rule, the analysis of experiments is based on Herring's relaxation mechanism [23]. Then for cubic crystals the relaxation rates of normal processes are given by the relations

$$\tau_{\mathrm{N}}^{(t)-1} = A_{\mathrm{N}}^{(t)} \omega T^4 , \tag{2.9a}$$

$$\tau_{\mathrm{N}}^{(l)-1} = A_{\mathrm{N}}^{(l)} \omega^2 T^3 . \tag{2.9b}$$

Detailed expressions for the relaxation rates in the case of Simons mechanism can be found in Refs [26, 27].

It should be emphasized that the use of Eqns (2.8) and (2.9) for $\tau_{\mathrm{U}}^{(i)-1}$ and $\tau_{\mathrm{N}}^{(i)-1}$ effectively restricts the applicability of the theory by the region of relatively low temperatures of the order of temperature $T_{\max}$ of the maximum thermal conductivity. And indeed, at $T > T_{\max}$ the exponential dependence on T for $\tau_{\mathrm{U}}^{(i)-1}$ must be replaced by the power-type dependence. At the same time, the dependence of $\tau_{\mathrm{N}}^{(i)-1}$ on T is also changed: $\tau_{\mathrm{N}}^{(i)-1} \sim T$.

In the above discussion we have neglected the contribution from optical modes. This problem is dealt with in Refs [28, 29] (see also Section 2.3).

The above formulas for thermal conductivity in the Callaway theory imply that the phonon spectrum can be described in the so-called single-mode approximation. Roughly speaking, the implication is that the heat is transferred mainly by the longitudinal modes. One can extend the theory to the case of crystals with highly anisotropic phonon spectrum and consider the partial contributions into $\varkappa$ from the modes of different polarization (see Section 2.2).

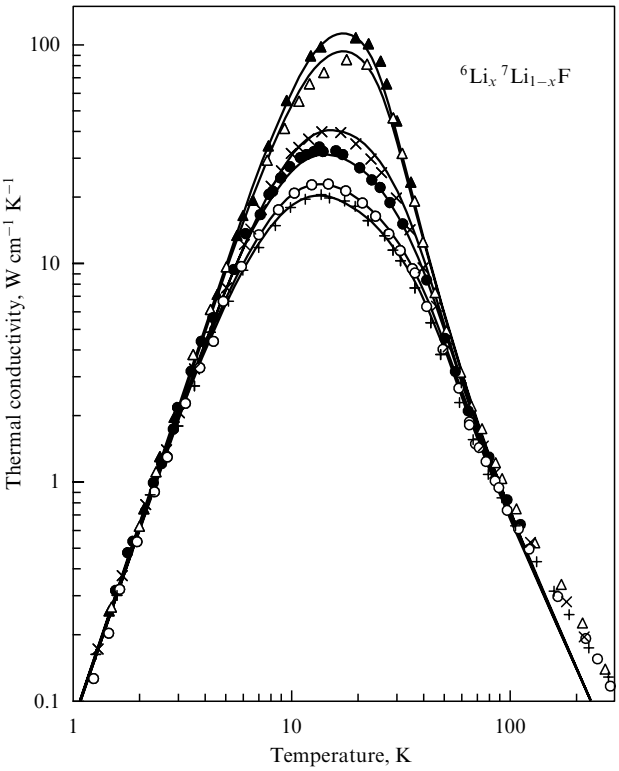

Figure 1. Thermal conductivity vs. temperature for LiF crystals with a different content of lithium isotope ^{6}Li: Δ — 0.01%, ▲ — 0.02%, × — 4.6 %, ○ — 25.0 %, + — 50.1%, • — 90.4%. Symbols represent experimental measurements; solid curves are calculated from the complete Callaway model. Data for the naturally occurring species (∼ 7.4% ^{6}Li) is not included, since they are close to those for the LiF specimen with 90.4% ^{6}Li ($L_{\mathrm{C}} = 0.51$ cm, $T_{\mathrm{D}} = 730$ K, $v_{\mathrm{s}} = 5.0 \times 10^6$ cm s^{-1}) [32].

2.1.2 Thermal conductivity of lithium fluoride. First experiments with controlled variation of the isotopic composition of crystals were done by Berman with colleagues [30] using lithium fluoride (LiF). The experimental results were interpreted in Ref. [31] based on the simplified Callaway model (without the additional term $\varkappa_2$). Satisfactory agreement was only obtained when the isotopic disorder parameter was five times the calculated value. Later on, the measurements with LiF were performed for a number of specimens with different content of lithium isotopes ^{6}Li and ^{7}Li (from 0.01 to 50%) in the broad temperature range from 1 to 300 K [32] (Fig. 1). The steady longitudinal heat flux method was used in the course of measurements, and the error in the definition of the absolute value of thermal conductivity did not exceed ∼ 5% for $T < 200$ K. It was found that in the neighborhood of maximum the thermal conductivity of chemically very pure crystals changes dramatically with the concentration of isotopes. This result was later confirmed by Thacher [33]. Theoretical analysis of measured data in Ref. [32] was performed using the complete single-mode Callaway model. The rate of isotope scattering was found by the Klemens formula (2.6b), with the exception of two isotopically most pure specimens in which the phonon scattering by the residual chemical impurities dominates over the scattering by isotopes. For this reason, the rate of scattering by point defects was selected so as to tally the calculated and the experimental values of thermal conductivity. The parameters of three-phonon scattering processes, as well as boundary and dislocation scattering, were determined by fitting the model in with the experimental data at low temperatures (below 100 K), and only one set of these parameters was used for all specimens. As seen from Fig. 1, the model selected gives adequate description of the experimental data at low temperatures. According to the complete Callaway model, the high sensitivity of thermal conductivity of very pure specimens to isotopic impurities is conditioned by the sharp concentration dependence of the additional term $\varkappa_2$ in the neighborhood of the maximum. Theoretical findings clearly illustrating this effect in LiF are presented in Fig. 2.

Unfortunately, the dependence of the relaxation rate τ_{iso}^{-1} of phonons on polarization vectors was not taken into account in Ref. [32]. Because of this, the description of τ_{iso}^{-1} is, generally speaking, not correct. The matter is that in the diatomic lattice of LiF with the much different masses of components, the light atoms of lithium (whose isotopic composition was varied) vibrate mainly in the optical modes. Their role in the formation of the acoustical part of the spectrum is not much pronounced. The corresponding effect on τ_{iso}^{-1} is just the one taken into account by the polarization vectors. Because of this, the quantitative estimates for the relaxation rates of thermal phonons in LiF need to be specified more exactly.

2.1.3 Thermal conductivity of diamond. Recently, the experimental data on thermal conductivity of diamonds with different isotopic composition were gathered [34 – 38]. Measurements were performed in the temperature range from 104 to 1200 K with different experimental techniques: optical

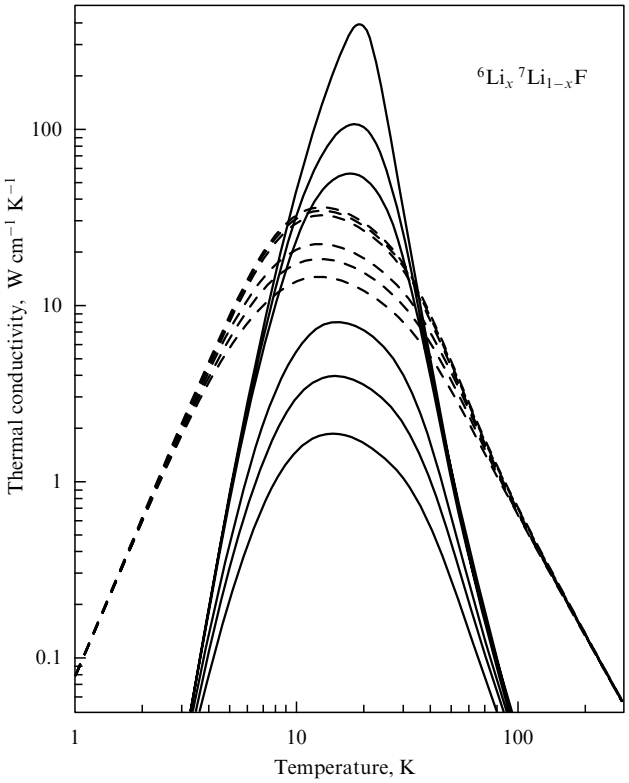

Figure 2. Temperature dependences of terms $\varkappa_1(T)$ and $\varkappa_2(T)$ of the total thermal conductivity of LiF in the complete Callaway model at different rates of isotope scattering: $\tau_{iso}^{-1} = A_{iso}T^4x^4$, $x = \hbar\omega/k_BT$. Solid lines represent $\varkappa_2(T)$, dashed lines $\varkappa_1(T)$. In both the families of curves, the top line corresponds to $A_{iso} = 0$; the transition at fixed temperature to the next line below corresponds to the increase of A_{iso} in the sequence 0.02; 0.05; 0.5; 1.0; 2.0 s^{-1} K^{-4} [32].

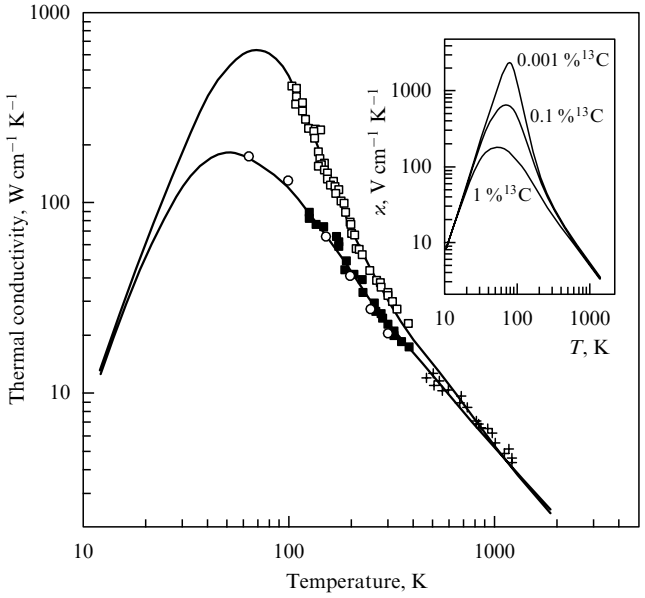

Figure 3. Temperature dependence of the diamond thermal conductivity. Points for natural isotopic composition (1.1% ^{13}C) are marked with black squares, and light squares mark the points for the enriched crystal (0.1% ^{13}C) [37]. The diagram also includes data from Ref. [39] (circles) and Ref. [38] (crosses). Solid lines are the result of fitting in the Callaway model [6] to the experimental data. Inset shows the results of model calculations of $\varkappa(T)$ for diamond crystals with different concentrations of ^{13}C.

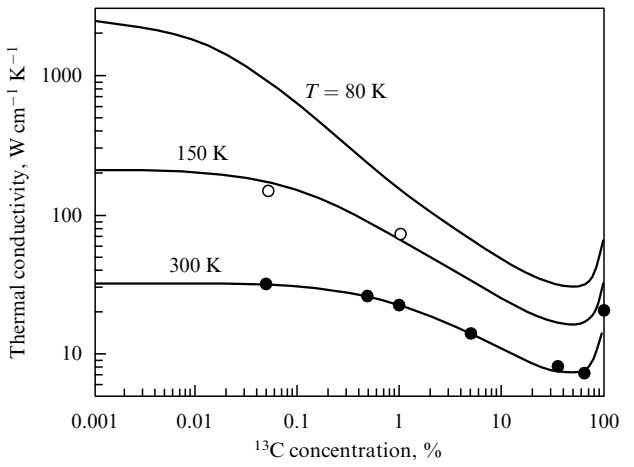

Figure 4. Diamond thermal conductivity vs. the concentration of ^{13}C isotope at different temperatures. Symbols denote experimental data; solid curves were calculated from the Callaway theory [37].

mirage [34, 37], pulse (optical or laser) heating [35, 36], and temperature wave (variant '3ω') [38]. They indicated that thermal conductivity of diamond enriched to 99.9% ^{12}C isotope is 50% higher than thermal conductivity of natural diamond (98.9% ^{12}C) and at room temperature is the highest among any natural or man-made materials. The temperature dependence of thermal conductivity of diamond crystals is shown in Fig. 3, and Fig. 4 displays thermal conductivity versus the concentration of ^{13}C isotope at fixed temperature.

In 1914, P Debye gave a qualitative explanation of the high thermal conductivity of diamond [40]. The reason is that diamond has exceptionally strong interatomic bonds, low atomic mass, and simple lattice structure with a weak anharmonism. According to the theory of Leibfried and Schlömann [41] (see also Ref. [39]), thermal conductivity at $T > T_D$ can be represented as

$$\varkappa(T) = BM\Omega^{1/3}\frac{T_D^3}{T\gamma^2},$$

where B is the constant that does not depend on the properties of the material, and γ is the Grüneisen constant. It immediately follows that the value of thermal conductivity is determined by the factor $M\Omega^{1/3}T_D^3$, the latter being the largest for crystals made up of light elements with strong interatomic bonds, inasmuch as the term T_D^3 dominates. Of all the solids it is diamond that has the highest Debye temperature $T_D \approx 1845$ K. Because of this, the room temperature for diamond is a low temperature, and hence the three-phonon processes with the quasi-momentum umklapp, which constrain thermal conductivity of most nonmetallic crystals at room temperature, are to a large extent 'frozen-out'. Thermal conductivity of diamond at room temperature, as opposed to many other materials, is mainly conditioned by the normal three-phonon processes and scattering from the lattice defects, including the 'impurity' isotopes.

The analysis of experimental data in the framework of the Callaway theory [6] was performed by Wei et al. [37] using the essentially single-mode approximation. It turned out that with proper selection of the frequency dependences for the

anharmonic processes it is possible to obtain good approximate formulas of thermal conductivity as a function of both the temperature and concentration (see Figs 3 and 4). A noticeable increase in thermal conductivity of isotopically enriched diamond at room temperature occurs against the background of considerable impact of normal processes on the phonon relaxation.

Using equations (2.24) that follow one can give a straightforward explanation of the considerable change in thermal conductivity of highly enriched diamond crystals at room temperature. Over this region $\tau_N \ll \tau_R$ and $\tau_C \to \tau_N$. In such a situation, expression (2.4) holds for thermal conductivity. This circumstance was noted in Refs [42, 43] (see also Ref. [5]). Then it is possible to explicitly single out the contribution to thermal resistance ΔW, associated with isotope scattering. Figure 5, reproduced from Ref. [42], illustrates the corresponding results of calculating thermal conductivity of diamond with different isotopic compositions in the single-mode approximation. We notice that the experimental data for the concentrations 0.07 and 0.5% ^{13}C is adequately explained by isotope scattering.

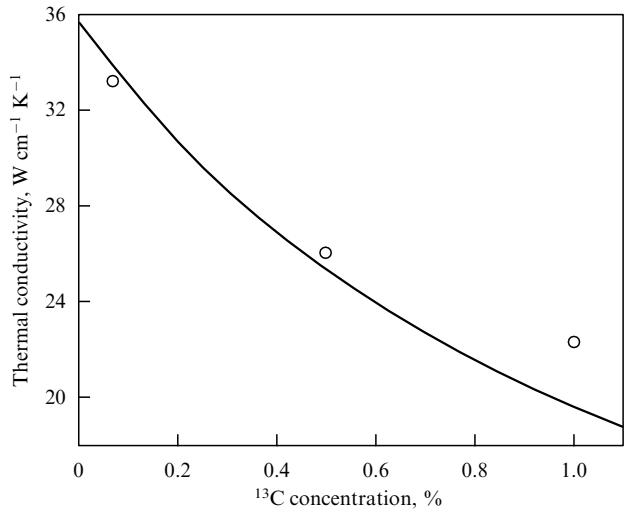

Figure 5. Diamond thermal conductivity vs. the concentration of ^{13}C isotope. Symbols denote experimental data [34]; solid curve is calculated [42]. $T = 300$ K, $T_D = 1845$ K, $v_s = 1.18 \times 10^6$ cm s^{-1}.

2.2 Extended Callaway model: anisotropic spectrum

2.2.1 Basic relations. In the case of crystals with highly anisotropic phonon spectrum, like germanium and silicon, owing to the difference in the dispersion of longitudinal and transverse branches of the phonon spectrum, the expressions for relaxation time and rate turn out to be essentially different for phonons of different polarizations. Because of this, for the description of crystal thermal conductivity at temperatures near the maximum of $\varkappa(T)$ and above, in place of the single-mode approximation one should rather use representations that explicitly take such an anisotropy into account. The generalized expression for $\varkappa(T)$ was proposed by Asen-Palmer et al. [44] in the context of theory [6]. The partial contributions from longitudinal (l) and transverse (t) modes were taken into consideration.

For a cubic crystal, in the case when the temperature gradient exists along one of the crystallographic axes, thermal conductivity is defined as follows

$$\varkappa = \varkappa_t + \varkappa_l \,, \tag{2.10}$$

$$\varkappa_i = \gamma_i \frac{k_B^4}{2\pi^2\hbar^3 v_i}\ T^3 \left[\langle \tau_C^{(i)} \rangle + \frac{\langle \tau_C^{(i)}/\tau_N^{(i)} \rangle^2}{\langle \tau_C^{(i)}/(\tau_N^{(i)}\tau_R^{(i)}) \rangle} \right] . \tag{2.11}$$

Here, $i = t, l$; v_i is the group velocity of sound, and γ_i is 2/3 or 1/3 for transverse and longitudinal modes, respectively. Angle brackets denote the following integral

$$\langle f_i \rangle = \int_0^{T_D^{(i)}/T} \frac{x^4 \exp x}{(\exp x - 1)^2}\, f_i(x)\, \mathrm{d}x \,,$$

where the upper limit is $T_D^{(i)} = \hbar\omega_i/k_B$, and ω_i is the Debye frequency for i-polarization.

Assuming that different relaxation mechanisms of non-equilibrium phonons act independently of one another, we find

$$\tau_R^{(i)-1} = \tau_b^{-1} + \tau_{iso}^{-1} + \tau_U^{(i)-1} \,. \tag{2.12}$$

In Eqn (2.12), τ_b, τ_{iso} and $\tau_U^{(i)}$ are the relaxation times of phonons due, respectively, to scattering by the sample boundaries, elastic scattering brought on by isotopic disorder, and inelastic anharmonic umklapp processes. Notice that the frequency dependence of the rate of transverse mode isotope scattering in germanium and silicon is, generally speaking, unconventional. Since $\tau_{iso}^{-1} \sim \omega^2\rho(\omega)$, in the domain of strong frequency dependence of t-modes the scattering rate changes faster than ω^4. For example, in the case of germanium the partial spectrum of these modes has a sharp peak at 2.4 THz. The spectrum of l-modes is localized here at much higher frequencies ~ 6 THz [45]. Nevertheless, since the theoretical lattice dynamics is described in Debye approximation, the rate τ_{iso}^{-1} was chosen in the form (2.6b). The parameters of isotope scattering have not been varied in the calculations.

Recall also that in the case when the N-processes proceed slower than the resistive processes of phonon scattering, it is the first term in Eqn (2.1) that dominates. Otherwise the thermal conductivity is determined by the second term.

2.2.2 Thermal conductivity of germanium and silicon. The effect of isotopic disorder on thermal conductivity was first discovered by Geballe and Hull [3], who found that thermal conductivity of germanium crystal enriched to 95.8% ^{74}Ge isotope is at maximum about 3 times as high as that of the germanium crystal with natural isotopic composition. The isotopic disorder parameter for the enriched specimen was about 15 times less than that for the specimen of natural origin. It is interesting to note that J Callaway in paper [6], where he formulated his theory of lattice thermal conductivity, provided quite a good theoretical description of experimental data gathered in Ref. [3] for the temperature range between 3 and 100 K using the single-mode approximation, with the exception of the region near the maximum of thermal conductivity. One of the main reasons for the discrepancy between the theory and experiment was the inadequate employment of the Debye model for germanium, which is a material with strong dispersion of transverse phonons. A similar situation is observed with silicon. Later on Holland [46] gave a good description of experimental data on germanium thermal conductivity in a broad temperature

range, including the results on the isotopically modified germanium from Ref. [3]. He used the model that only included the 'regular' term $\varkappa_1(T)$ (thus disregarding the normal processes) with separate contributions from the different phonon branches. Because of this, his magnitudes for the relaxation times are wrong. The high-precision measurement results on thermal conductivity of germanium crystals with different isotopic compositions, including the nearly monoisotope sample in ^{70}Ge with the enrichment of 99.99%, were reported recently in Ref. [47] over a broad temperature range from 2 to 300 K (Fig. 6). Measurements were performed with samples having the shape of rectangular parallelepipeds with sizes $0.25 \times 0.25 \times 4.0$ cm, using the steady-state longitudinal heat flux method. The measurement error in the absolute value of thermal conductivity did not exceed 2% for $T < 200$ K. For the isotopically pure germanium sample (99.99% ^{70}Ge), the thermal conductivity at maximum is about 110 W cm^{-1} K^{-1} at the temperature of 15 K, which is greater by a factor of approximately 8.1 than the corresponding value for germanium of natural isotopic composition. Hence it follows that in natural germanium at temperatures near the thermal conductivity maximum the thermal resistance is practically entirely (by 85%) determined by phonon scattering from isotopes. At room temperature, thermal conductivity of ^{70}Ge sample is 20% higher than that of natural germanium, and within experimental accuracy it coincides with the appropriate magnitude of the specimen with 96.3% ^{70}Ge.

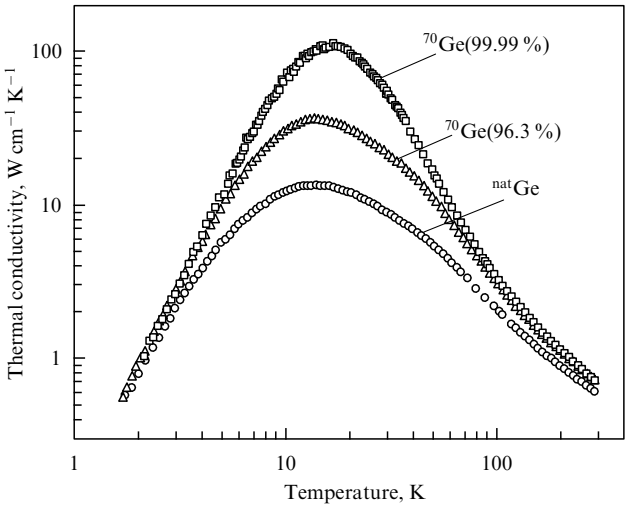

Figure 6. Thermal conductivity vs. temperature along the [100] axis of germanium single crystals with different isotopic compositions [47]; $L_C = 0.28$ cm, $T_D = 375$ K, and $v_s = 3.5 \times 10^5$ cm s^{-1}.

Measurements of $\varkappa(T)$ performed with a unique crystal (99.99% ^{70}Ge) and with other germanium crystals with controlled isotopic composition allowed the researchers to study in detail the isotope effect on thermal conductivity [44, 47]. The parameters of studied specimens are given in Tables 1 and 2.

Description of boundary and isotope scattering in Ref. [44] was based on equations (2.5) and (2.6). It turned out that in the context of extended Callaway model the temperature dependence of crystal thermal conductivity can be adequately described using one and the same set of fitting parameters for anharmonic processes for all germanium specimens. Namely, it was found that

$$A_N^{(t)} = 2 \times 10^{-13}\ \mathrm{K}^{-4}, \quad A_U^{(t)} = 1 \times 10^{-19}\ \mathrm{K}^{-4},$$
$$A_N^{(l)} = 2 \times 10^{-21}\ \mathrm{s\,K}^{-3}, \quad A_U^{(l)} = 5 \times 10^{-19}\ \mathrm{s\,K}^{-3}, \quad (2.13)$$
$$B^{(t)} = 55\ \mathrm{K}, \qquad B^{(l)} = 180\ \mathrm{K}.$$

The values of $B^{(i)}$ correlate with the Debye temperatures for t and l modes, and to an order of magnitude are equal to $T_D^{(i)}/2$.

Figure 7 shows experimental data for germanium samples with different isotopic compositions and the results of theoretical fitting using the extended Callaway model — that is, with separated contributions from different phonon polarizations for both the regular term $\varkappa_1$ and the additional term $\varkappa_2$.

According to the results obtained for the partial relaxation times, over the entire temperature range the behavior of $\varkappa(T)$ is essentially determined by the normal anharmonic processes. The inclusion of U-processes proceeded with the participation of longitudinal modes allows one to correctly describe the decline of thermal conductivity to the right of the maximum. The inclusion of partial contributions from t and l modes into $\varkappa(T)$ also permits description of the nontrivial change in the location of the maximum of crystal thermal conductivity as the isotopic composition is varied (see Section 2.2.3).

Observe also that the description of experimental data using the common set of parameters in the region of the maximum of $\varkappa(T)$ at $T \sim T_{max}$ for the highly enriched samples is not so good as that for the specimen with natural isotopic composition and the specimen containing 50% ^{70}Ge and 50% ^{76}Ge. This is apparently related to the fact that at $T \sim T_{max}$ there occurs interference between the process of scattering by isotopes and the anharmonic process of phonon scattering, whereas the Callaway theory treats the different scattering processes as independent ones.

Table 1. Isotopic composition of germanium specimens studied in Refs [44, 47].

Specimen	^{70}Ge, %	^{72}Ge, %	^{73}Ge, %	^{74}Ge, %	^{76}Ge, %	ξ^2, 10^{-5}	M, a.m.u.
^{70}Ge(99.99)	$\geqslant 99.99$	$\leqslant 0.01$	0.00	0.00	0.00	0.008	69.924
^{70}Ge(96.3)	96.3	2.1	0.1	1.2	0.3	7.75	70.035
^{70}Ge(95.6)	95.6	3.8	0.0	0.6	0.0	4.84	70.02
^{74}Ge	0.7	1.1	1,6	95.8	0.8	3.69	73.87
^{76}Ge	0.0	0.1	0,2	13.7	86.0	8.76	75.64
^{nat}Ge1	21.23	27.66	7.73	35.94	7.44	58.9	72.59
^{nat}Ge2	21.23	27.66	7.73	35.94	7.44	58.9	72.59
$^{70/76}$Ge	43	2	0	7	48	154	73.12

Table 2. Geometry of germanium specimens studied in Refs [44, 47]. (Symbol O denotes the crystallographic axis whose direction is close to the longer edge of the specimen; I is the angle between the edge and the axis in degrees.)

Specimen	O/I	a, mm	b, mm	l, mm
^{70}Ge(99.99)	100/6	2.20	2.50	40
^{70}Ge(96.3)	100	2.50	2.50	40
^{70}Ge(95.6)	110/27	1.25	1.49	14
^{74}Ge	100/0	1.57	1.30	25.4
^{76}Ge	100/2	1.27	2.54	35
^{nat}Ge1	100/0	2.46	2.50	40
^{nat}Ge2	100/0	1.30	1.30	15
$^{70/76}$Ge	110/11	2.02	2.00	23

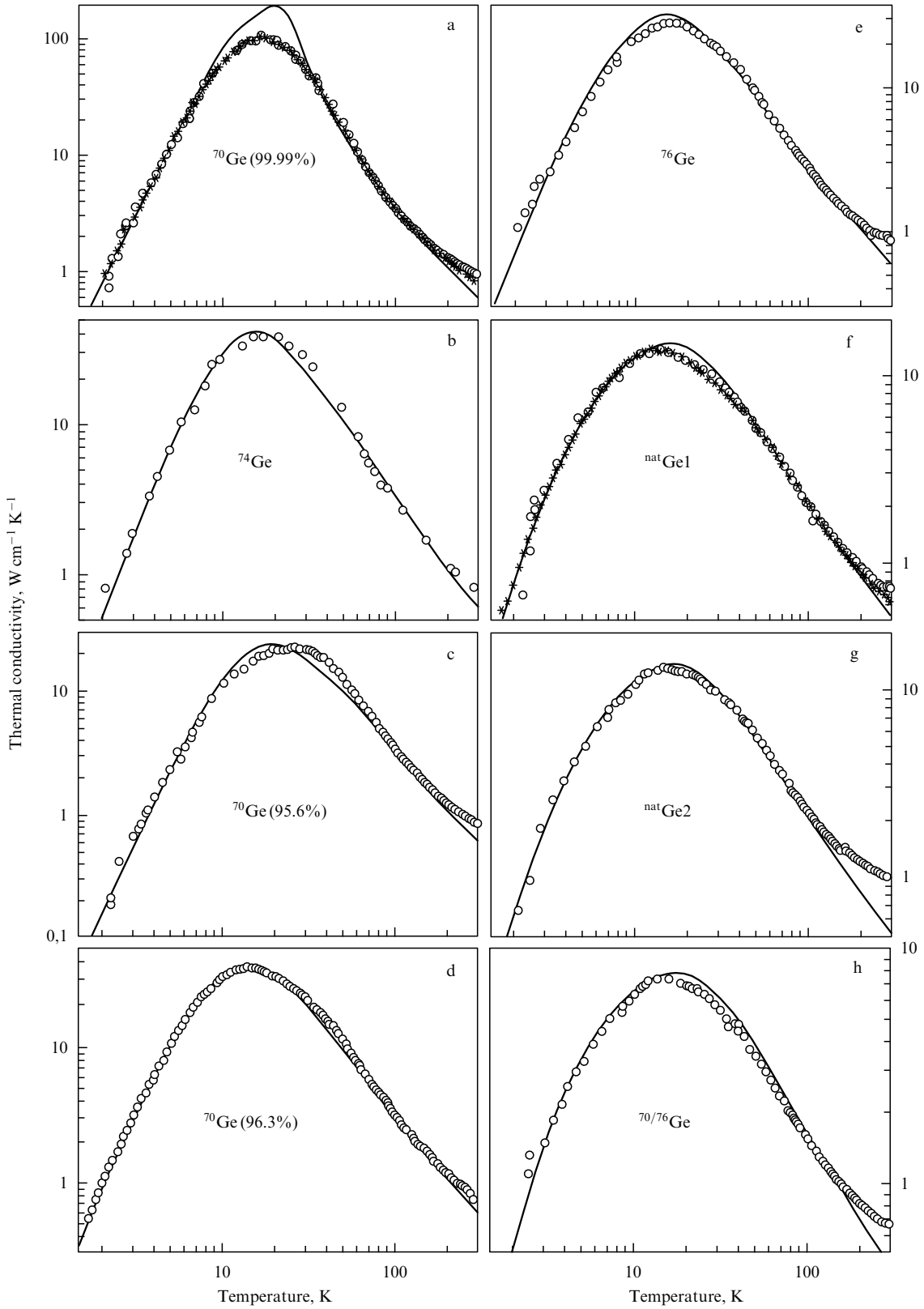

Figure 7. Thermal conductivity of germanium single crystals with different isotopic compositions. Symbols denote experimental data; solid curves are theoretical results [44]. Experimental data for the ^{74}Ge sample were taken from Ref. [3].

The measurements of thermal conductivity of bulk silicon crystal isotopically enriched to 99.86% ^{28}Si were reported in Ref. [48]. Thermal conductivity was measured by the steady-state longitudinal heat flow method with rod-shaped specimens over the temperature range from 2 to 310 K. The specimen enriched with ^{28}Si isotope had an average diameter of 0.237 cm and a length of about 3 cm, while the corresponding dimensions of the specimen with natural isotopic composition were 0.245 and ~ 2.6 cm. The experimental results obtained are shown in Fig. 8. The same figure

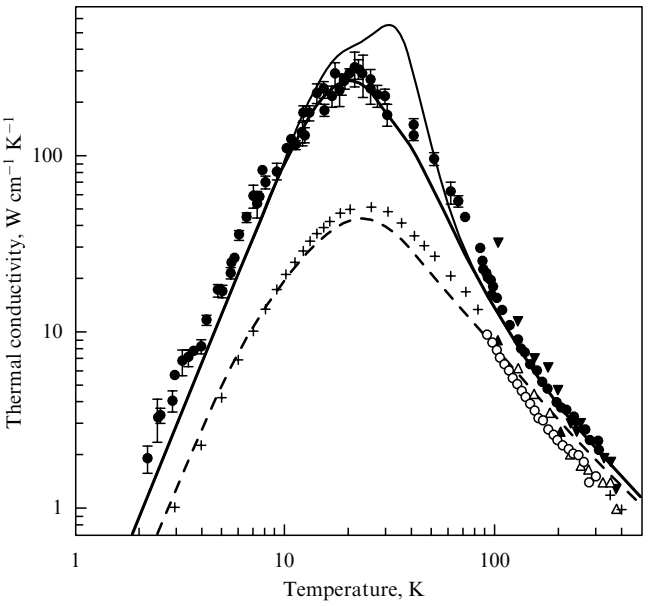

Figure 8. Isotope effect in the silicon thermal conductivity [48]: • and ○ — experimental data for bulk silicon single crystals isotopically enriched to 99.86% ^{28}Si, and natural silicon; ▼ and Δ — experimental data for films of ^{28}Si and natural Si from Ref. [49]; × — recommended values for natural silicon from handbook [50]. Thin solid and dashed lines denote theoretical results for ^{28}Si and natural Si from Ref. [49]. Thick solid line shows the calculated result based on the same model and produced using the real parameter $\xi^2 = 2.33 \times 10^{-6}$ for a silicon specimen with high concentration of ^{28}Si. For natural Si, the parameter is $\xi^2 = 201 \times 10^{-6}$.

also demonstrates the data on thermal conductivity of thin silicon films with different isotopic compositions, measured earlier in Ref. [49] by an optical pump-and-probe method. The data obtained by different methods coincide at the higher temperatures, but in the vicinity of 100 K, where the optical measurements are less reliable, the discrepancy is quite considerable. According to the authors of paper [48], the experimental accuracy for bulk specimens is within 10%, with the exception of the neighborhood of the maximum of thermal conductivity, where the error may be as large as 25%.

We emphasize the unexpectedly high experimental values of thermal conductivity of the isotopically enriched bulk silicon crystal. At maximum, for example, the thermal conductivity of an enriched crystal is approximately 6 times that of natural silicon, and at room temperature it is 60% higher than the thermal conductivity of natural silicon. We believe that there results call for independent verification.

As already indicated, for germanium and silicon, according to neutron experiments in units of ion plasma frequency, the phonon dispersion curves are very close throughout the entire volume of Brillouin zone [51]. On the basis of theoretical estimates, the parameters of the effective force interaction are also close in magnitude. This allows determination of the parameters of the anharmonic relaxation processes for silicon using the results for germanium. Here in the first place we ought to take into account the renormalization of the effective Debye temperatures: $T_D(\mathrm{Si})/T_D(\mathrm{Ge}) = 1.75$. In addition, we note that the parameter A_N is defined in the following way

$$A_N \propto \frac{\gamma^2}{Ma^2 T_D^5} .$$

Taking advantage of the closeness of the effective Grüneisen parameters, the lattice constants and the force constants, we find that $A_N(\mathrm{Si})/A_N(\mathrm{Ge}) \approx (M_{\mathrm{Si}}/M_{\mathrm{Ge}})^{3/2}$. In other words, for estimates we only need to take into consideration the distinction between the masses of germanium and silicon atoms. As far as the parameter A_U is concerned, its dependence on T_D is determined by the following circumstance. Namely, the matrix element squared for the anharmonic phonon process must be proportional to the product of energies of the corresponding modes. Then two of the three phonons have the energy of the order of $T_D^{(i)}$, and so $A_U^{(i)} \propto T_D^{(i)-2}$. This procedure for finding the anharmonic parameters of silicon allowed the researchers to provide a satisfactory description of experimental findings for the samples of natural composition and those enriched to 99.9% ^{28}Si [48, 49].

We also used the values of anharmonic parameters (2.13) quoted above for discussing the experimental results on germanium thermoelectric power (see Section 3).

2.2.3 Thermal conductivity of germanium near the maximum. Figure 9 gives theoretical data that illustrate the temperature dependence of thermal conductivity of *t*- and *l*-modes in germanium crystals with different isotopic compositions. The curves pass through the maxima at $T_{\max}^{(l)} = 18$ K and $T_{\max}^{(t)} = 12$ K for the ^{70}Ge (99.99%) specimen. In this situation, the main contribution to $\varkappa(T)$ directly at maximum of total thermal conductivity is associated with the *l*-modes. The contributions from 'fast' long-wave (t_1) and 'slow' short-wave (t_2) transverse phonons are comparable. However, in the thermal conductivity of the ^{70}Ge(96.3%) specimen it is the t_1-modes that dominate, because the contributions from *l*-modes and t_2-modes are to a large extent suppressed because of the isotope scattering. This circumstance also accounts for the decrease of the temperature at the maximum of the curve by ~ 4 K for ^{70}Ge(96.3%) as compared with ^{70}Ge(99.99%) [52]. In the case of natural germanium, in the situation of sufficiently strong isotope scattering, the role of *l*-modes slightly increases compared to *t*-modes, and the maximum shifts by fractions of kelvin towards the higher temperatures.

Figure 8 shows theoretical data for silicon with the high concentration of ^{28}Si, reproduced from paper [49]. The

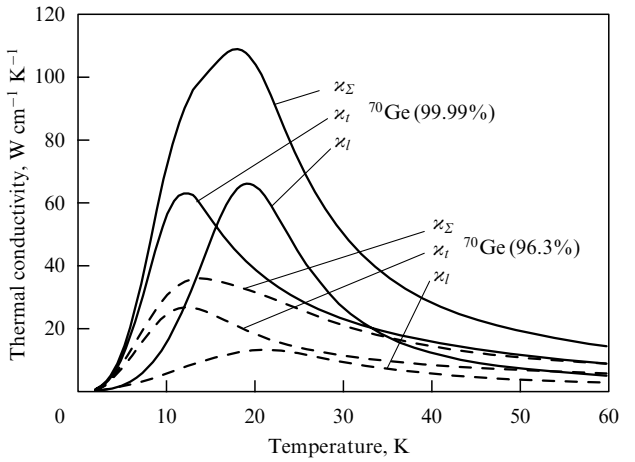

Figure 9. Contributions of transverse and longitudinal phonons to the thermal conductivity of germanium single crystal with the enrichment to 99.99% ^{70}Ge (solid lines) and 96.3% ^{70}Ge (dashed lines) [52].

procedure of their obtaining is described in Section 2.3. For silicon, the effective Debye temperature is 1.75 times as high as that for germanium. Because of this, the temperatures $T_{\max}^{(l)}$ and $T_{\max}^{(t)}$ of the maxima of partial thermal conductivities are higher by about 10 K.

Attention is drawn to the fact that the location of the maximum of thermal conductivity depends considerably on the quality of surface finishing. For germanium, the role of diffuse and mirror scattering of phonons at the specimen boundaries was analyzed in Refs [44, 53]. In perfect highly enriched specimens at $T \geqslant 4$ K, the phonon flow deviates from the Knudsen pattern, when the collisions are mostly with the walls. These deviations were explained (and supported with quantitative estimates) with reference to the fact that the phonon gas starts to feature the viscous Poiseuille flow [53]. The crux of a matter is that in the case of rather perfect monoisotopic crystals the effects of static defects and isotopic disorder on the structure of the nonequilibrium phonon distribution function is disguised by the anharmonic N-processes. In such a case, only the processes of phonon scattering by the walls of the specimen are resistive. However, owing to the more frequent nonresistive N-processes the transport mean free path of phonons increases effectively as $\sim d^2/l_{\mathrm{N}}$. Earlier, the switch to the Poiseuille flow was clearly observed only in crystals of solid helium. The issue of the manifestation of the hydrodynamic regime in connection with the problem of second sound has been analyzed for NaF and Bi crystals, in which the mechanism of isotope scattering is not present. The corresponding results are discussed in the book by Berman [17].

2.2.4 Effects of isotopic disorder on the phonon scattering umklapp processes. In the theoretical analysis of the experiments in the context of an extended Callaway model we assumed above that different processes of nonequilibrium phonon scattering are independent. In general, the description of experiments is fairly satisfactory. However, a systematic discrepancy was discovered in Ref. [44] between the theory and experiment to the right of the maximum of thermal conductivity for isotopic mixtures of germanium, namely, for the natural composition and for the specimen with the ultimate isotopic disorder, containing ^{70}Ge and ^{76}Ge isotopes in 50/50 proportion.

Using relations (2.10)–(2.12), we additionally analyzed the experimental results for the temperatures below 60 K and refined the values of parameters governing inelastic anharmonic phonon scattering. It turned out that as the isotopic disorder (i.e. the parameter ξ^2) increases, the intensity of anharmonic umklapp processes also enhances. Then the exponential factor B in expression (2.8) for the relaxation rate τ_{U}^{-1} decreases, and the preexponential factor A increases. This result may be interpreted as follows. In a regular monoisotopic lattice over the temperature range where the inelastic U-processes freeze out, the stationary momentum distribution $\Phi(\mathbf{q})$ of phonons must be *anisotropic*. This is because the nonequilibrium phonons, in accordance with the variational principle, must leave those regions of the Brillouin zone where their scattering is most efficient. In crystals with *isotopic* disorder, the elastic *isotropic* scattering by isotopes suppresses the anisotropy of the distribution $\Phi(\mathbf{q})$, making it 'more isotropic'. As a result, the intensity of U-processes enhances with the increasing parameter ξ^2.

Recall that the problem of the specific role of the longitudinal long-wave phonons in crystal thermal conductivity was raised already in work [54]. In Ref. [23] (see also book [9]), it was demonstrated that in real anisotropic crystals there are certain regions in the quasi-momentum space, in which such l-phonons may decay through the processes of the type $l + t' \to t''$. For t-modes such processes are also possible in the case of an isotropic system. Then, according to the variational principle, in the ideal system the nonequilibrium phonons must be distributed in the Brillouin zone in such a way as to partly suppress the role of the above processes. It is interesting that, according to our results, the transition from the practically regular ^{70}Ge(99.99%) specimen to isotopically contaminated samples shortens the lifetime of l-modes more considerably than that of t-modes.

In this way, the analysis of experimental data for germanium crystals with different isotopic compositions reveals that in the neighborhood of the maximum of thermal conductivity the intensity of the anharmonic umklapp processes increases with the parameter of isotopic disorder ξ^2. This means that — at least near the thermal conductivity maximum — the elastic phonon scattering due to isotopic disorder and inelastic anharmonic scattering umklapp processes are not independent.

2.3 Variational method

2.3.1 Variational principle. In the framework of the kinetic equation, the consistent theory of phonon thermal conduction was constructed by J Ziman based on the variational principle. This theory is presented in his classical monograph [9], and has not lost its relevance ever since.

The kinetic equation in this theory is linearized by replacing in the field term the occupation numbers $n(l)$ for the phonon modes by their equilibrium values $n_0(l)$ ($l \equiv \{\mathbf{q}, j\}$). Simultaneously, the function $\Phi_\alpha(l)$ characterizing small deviations from equilibrium appears in the collision integral. To the lowest order with respect to the temperature gradient we get

$$n(l) = n_0(l) + \Phi_z(l) n_0(l)\bigl[n_0(l) + 1\bigr] \frac{\partial T_z}{\partial z}\,. \tag{2.14}$$

The function Φ_z therewith satisfies the equation of the form

$$X_z(l) = -\sum_{j'} \int \mathrm{d}\mathbf{q}' P(l, l')\, \Phi_z(l')\,, \tag{2.15}$$

where

$$X_z(l) = \frac{\hbar\omega(l)}{k_{\mathrm{B}} T^2}\; n_0(l)\bigl[n_0(l) + 1\bigr] v_z(l)\,. \tag{2.16}$$

The factor $P(l, l')$ is the matrix element of the operator of scattering taken over states l and l'. According to the principle of microscopic reversibility, one finds $P(l, l') = P(l', l)$. In our present case the operator P consists of three terms which describe the phonon scattering by the boundaries of the specimen, the anharmonic interaction, and the effect of isotopic disorder.

Let us write out explicitly that part of $P(l, l')$ which characterizes the isotope scattering. Then we have [20]

$$\delta P(l, l') = \frac{\Omega_0 \xi^2}{8\pi^2}\; \omega(l)\omega(l')\bigl|e(l)e(l')\bigr|^2 n_0(l)\bigl[n_0(l') + 1\bigr] \times \delta\bigl[\omega(l) - \omega(l')\bigr]\,. \tag{2.17}$$

The thermal conductivity is given by the equality

$$\varkappa(T) = -\frac{k_B T^2}{8\pi^3} \sum_j \int \mathrm{d}\mathbf{q}\, \chi(l)\, \Phi(l)\,. \tag{2.18}$$

Following Ziman, we define the thermal resistance $W = 1/\varkappa$ in the form

$$W = \frac{8\pi^3}{k_B T^2} \frac{\sum_{jj'} \iint \mathrm{d}\mathbf{q}\ \mathrm{d}\mathbf{q}'\, \Phi(l)\, P(l,l')\, \Phi(l')}{\left(\sum_j \int \mathrm{d}\mathbf{q}\, X(l)\Phi(l)\right)^2}\,. \tag{2.19}$$

Observe that, in accordance with the variational principle, the function $\Phi_z(l)$ satisfying the kinetic equation (2.15) realizes the minimum of expression (2.19).

As a rule, the trial function is selected in the form of expansion over a given set of functions $\{\varphi_r\}$ with the coefficients η_r that have to be found. The corresponding set of equations in η_r takes the form

$$X_r = \sum_{r'} P_{rr'} \eta_{r'}\,, \tag{2.20}$$

where X_r and $P_{rr'}$ are the matrix elements of the operators X and P in the set of functions $\{\varphi_r\}$. The procedure for selecting the functions in the moments method is described in Appendix A.

2.3.2 Thermal conductivity of germanium and silicon. Results obtained by solving the kinetic equation. In the case of germanium and silicon crystals, to the best of our knowledge there are only two papers [55] and [56] in which the Ziman theory was applied for calculating the microscopic thermal conductivity. Interesting and informative calculations for germanium were carried out by Hamilton and Parrott [55] with detailed consideration of the role of the different types of anharmonic N- and U-processes ($t + t \to l$, $t + l \to l$, $l + l \to l$). At the same time, phonon scattering by boundaries and isotopes was also taken into account. The isotropic continual model was used by the authors for the analytic description of both the phonons and the anharmonic interaction. The contribution from the optical modes was not analyzed. The kinetic equation was solved in the multimoment approximation, assuming that

$$\Phi_z(\mathbf{q}, j) = -q_z \sum_{r'} \eta_{r'}^j \left(\frac{q}{q_D}\right)^{r'}\,.$$

A few first terms were retained in the power series expansion in moments.

According to results obtained in work [55], the dominant role in the thermal conductivity of germanium is played by the transverse phonons. In the temperature range to the right of the maximum, the contributions from N- and U-processes become equivalent already at the temperatures close to 60 K. As the temperature further increases, the umklapp processes start to dominate. The contribution from isotope scattering at different temperatures was also determined in this study for germanium crystal with natural isotopic composition.

Thermal conductivity of germanium and silicon crystals with different isotopic compositions was also studied in great detail in Ref. [12]. The authors developed the model of anisotropic pair interatomic interaction and used it for describing the phonon spectra, thermal expansion, and anharmonic interaction of phonons. The kinetic equation was solved by the iterative method. In doing so the role of acoustical and optical modes of longitudinal and transverse types was analyzed in detail. It was found that to the right of the maximum the contributions from the acoustical t- and l-modes into $\varkappa(T)$ are of the same order of magnitude. The contribution from the optical modes into relaxation of acoustic phonons becomes important already at $T \geqslant 100$ K, which agrees with the results of work [56] (see Table 3). For natural germanium, the contributions from phonon scattering by the boundary and by the isotopes are small, about 10% of the total thermal resistance at 100 K, and 3% at 300 K.

Table 3. Thermal conductivity (W cm^{-1} K^{-1}) of germanium with a natural isotopic composition. $\varkappa_{all}$ is the thermal conductivity with the inclusion of contributions from both acoustic and optical phonons to the three-phonon processes; $\varkappa_{b+iso}$ is the thermal conductivity with due account of only scattering by the boundaries and by the isotopes; $\varkappa_{acoust}$ is the thermal conductivity disregarding the scattering by optical phonons [12].

T, K	10	20	30	40	60	80	100	300	500	900
$\varkappa_{all}$	9.9	10.3	8.6	6.78	4.63	3.08	2.21	0.55	0.31	0.16
$\varkappa_{b+iso}$	10.0	12.1	14.5	16.1	17.7	18.3	19.5	23.0	23.4	24.1
$\varkappa_{acoust}$	9.9	10.3	8.6	6.78	4.90	3.52	2.49	0.85	0.52	0.29

As indicated above, measurements of thermal conductivity of thin silicon films with different isotopic compositions in the temperature range from 100 to 375 K were performed recently in Ref. [49] for the first time. Theoretical analysis of the data under consideration was carried out in Ref. [56]. The contribution to thermal resistance due to the isotope scattering was evaluated using relations (2.19) and (2.17). It is significant that the calculations have been performed based on the real spectrum of phonons and, which is most important, the sensible form of the distribution function Φ of nonequilibrium phonons. In the first place, the authors used the function Φ in the standard form

$$\Phi_z(l) \propto q_z\,. \tag{2.21}$$

Selected in this way, however, the function Φ is not periodical, and fails to correctly describe the contribution from the optical phonons (for which the group velocity may be negative). Generally speaking, the form of Φ that satisfies the necessary requirements is the following

$$\Phi_z(l) \propto \omega(l) v_z\,. \tag{2.22}$$

Figure 10 depicts four theoretical curves and the experimental data from Ref. [56]. Curves A and B, C and D were plotted using the phonon distributions in the forms (2.21) and (2.22) with and without regard for the contributions from optical phonons. It is interesting that fairly reasonable agreement with the experiment at $T = 250 - 300$ K occurs when Φ_z is selected in the form of relation (2.22), when the contribution from optical phonons is taken into account (and turns out to be quite considerable). At $T \leqslant 240$ K, the agreement with the experiment is not satisfactory. Observe that in the context of the isotropic continuum approximation [9] at $T \geqslant T_D$, when

$$\Delta W = \frac{9\pi\Omega_0 \xi^2 T_D}{14\hbar\, v_s^2}\,, \tag{2.23}$$

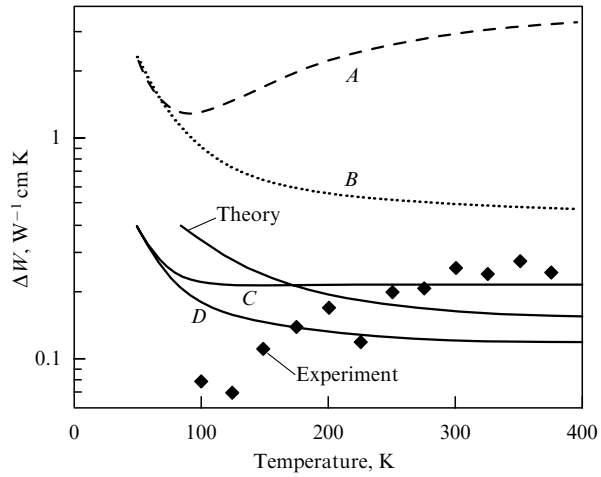

Figure 10. Thermal resistance of silicon due to isotope scattering as a function of temperature. Symbols denote experimental results from Ref. [49]; solid line ('theory') shows the results of calculations using the Ziman theory in the Debye approximation. Curves *A* and *B* correspond to the stationary distribution of nonequilibrium phonons in the form $\Phi \propto q_z$, with and without regard for the contribution from optical phonons. Curves *C* and *D* correspond to the distribution $\Phi_j \propto \omega(l) v_z(l)$, again with and without allowance for the contribution from optical modes.

it is also possible to qualitatively describe the scale of variation due to isotope scattering.

In the context of the variational procedure we have also analyzed the experimental data obtained for germanium in the range of relatively high temperatures. The corresponding results for thermal conductivity $\varkappa$ and the contribution from the isotope scattering mechanism to thermal resistance ΔW are presented in Table 4.

Table 4. Thermal conductivity $\varkappa$ (W cm^{-1} K^{-1}), and thermal resistance ΔW (W^{-1} cm K) due to the isotope scattering in germanium crystals.

T, K	ξ^2						
	8×10^{-8}	7.75×10^{-5}		58.9×10^{-5}		154×10^{-5}	
	$\varkappa$	$\varkappa$	ΔW	$\varkappa$	ΔW	$\varkappa$	ΔW
300	0.697	0.695	0.004	0.590	0.260	0.537	0.43
250	0.862	0.844	0.029	0.795	0.258	0.628	0.44
200	1.14	1.105	0.028	0.889	0.248	0.753	0.45
150	1.70	1.62	0.030	1.230	0.223	0.981	0.43

As in the above-considered case with silicon, the contribution into thermal resistance due to isotope scattering was evaluated with the aid of relations (2.19) and (2.17). The phonon spectrum was described using the bond-charge model in the version presented in Ref. [57]. Earlier we applied this model to studying the effects of isotopic composition on the lattice constant and the linear thermal expansion coefficient in the case of germanium and silicon [58, 59]. Calculations were performed employing the representation $\Phi_j \propto \omega(l)\, v_z(l)$ for the nonequilibrium part of the phonon distribution function, with and without regard for the contribution from optical modes.

We found that the value of ΔW was 0.20 W^{-1} cm K without regard for the contribution from the optical modes, and 0.32 W^{-1} cm K when this contribution was taken into account. The experimental value of ΔW is 0.26 W^{-1} cm K.

Note also the interesting result that follows from the data presented in Table 4. We found that at $T = 150$, 200 and 250 K the points for the impurity-related part of thermal resistance ΔW for ^{70}Ge (96.3%) specimens and those of the natural isotopic composition within the experimental accuracy fall on the straight line passing through the origin of coordinates. In other words, the relation $\Delta W \sim \xi^2$ holds true. At the same time, the data for the $^{70/76}$Ge specimen (with 50/50 proportion) do not fall on the straight line. The experimental values of ΔW are much lower than the theoretical values. Recall that a similar situation was encountered in the analysis of spectra of neutron inelastic scattering. It is possible that in the case of $^{70/76}$Ge mixture the deviation of ΔW from a linear dependence is caused by the effect of local ordering of light and heavy isotopes.

The results of Refs [12, 44, 55, 56] indicate that to the right of the maximum of $\varkappa(T)$ at temperatures $T \geqslant T_D/6$, the anharmonic processes of scattering of different types (i.e. U- and N-processes simultaneously) are effective, and the heat transfer therewith involves all groups of phonons. The influence of isotope scattering is not too large. Such a situation, in principle, does not give any good reason for the existence in the Brillouin zone of certain 'hot' domains within which the nonequilibrium phonons are scattered most efficiently through the anharmonic interaction. Accordingly, the standard Ziman distribution $\Phi_z(l) \propto q_z$ should give a satisfactory description of the real phonon distribution with respect to momenta. Then, however, according to the theory, the contribution from the isotopes into thermal resistance must actually be described by relations (2.17), (2.19). To get an estimate, one can use the formulas that correspond to the case of isotropic continuum and only take into account the contribution from the acoustic modes. We have at this rate

$$W = \frac{\pi \Omega_0\, \xi^2 T_D^{(i)}}{2\hbar\, v_s^2}\, \frac{T_D^{(i)}}{T}\, \frac{\sum_j (v_D/v_j)^2 (T/T_D^{(j)})^6 J_8^{(j)}(T_D^{(j)}/T)}{\sum_j \left((T/T_D^{(j)})^3 J_4^{(j)}(T_D^{(j)}/T)\right)^2}\,,$$

$$J_n^{(j)}\left(\frac{T_D^{(j)}}{T}\right) = \int_0^{T_D^{(j)}/T} \mathrm{d}x\, \frac{x^n \exp x}{(\exp x - 1)^2}\,. \qquad (2.24)$$

2.4 Lifetime of high-frequency phonons

Klemens [60] called attention to the fact that in isotopically pure silicon, even though the calculations of thermal conductivity due to thermal phonons featured slow growth, the mean free path of high-frequency 'superthermal' phonons may increase considerably at $T < T_{max} \approx 22$ K. This effect is due to the following circumstances. The rate of scattering by isotopes, according to Eqn (2.6b), is proportional to the phonon frequency to the fourth power. The conventional heat transfer is dominated by phonons with frequencies corresponding to the temperature energy equivalent of $4T$ — that is, at 20 K the heat is mainly transferred by phonons with an energy of about 80 K. If the energy supply to the silicon crystal (for example, under illumination with laser) gives rise to high-frequency phonons at the boundary of the Brillouin zone with the energy of ~ 220 K, then isotopes may reduce their mean free path by a factor of 60 (!) as compared with the mean free path of thermal phonons. Such a problem of propagation of high-frequency phonons in silicon and germanium crystals was considered by Maris [61]. The effects of elastic scattering by isotopes on the propagation of acoustic phonons in silicon were the subject of theoretical analysis by Tamura et al. [62].

3. Thermoelectric power of semiconductors with isotopic disorder

3.1 Phonon-drag thermopower

Classification of thermoelectric phenomena is usually based on the phenomenological transport theory. Let the specimen, in addition to the electric field, have also the temperature gradient. It has been known that the components of vectors of current density j_i and heat flux density q_i are expressed in terms of the components of vectors of temperature gradient $\partial T/\partial x_k$ and the generalized electric field $\mathbf{E}' = \mathbf{E} + \nabla\mu/e$, where μ is the chemical potential of charge carriers. We have (see, for example, book [9]) the following relationships

$$j_i = \sigma_{ik} E'_k - \varepsilon_{ik} \frac{\partial T}{\partial x_k}, \tag{3.1}$$

$$q_i = \pi_{ik} j_k - \varkappa_{ik} \frac{\partial T}{\partial x_k}. \tag{3.2}$$

Here σ_{ik}, ε_{ik}, π_{ik}, and $\varkappa_{ik}$ are the components of tensors of electric conductivity, thermoelectric power, Peltier coefficient, and thermal conductivity. Also, $i, k = x, y, z$ and summation is taken over the twice repeating Cartesian indices. Recall that if the total electric current in the specimen is zero and there exists the temperature gradient $\nabla T \neq 0$, then thermoelectric field $E'_i = \sigma^{-1}_{im} \varepsilon_{ik} \partial T/\partial x_k$ is generated (the Seebeck effect, $Q = \sigma^{-1}\varepsilon$ is the thermopower). Alternatively, if the temperature is kept constant along the specimen ($\nabla T = 0$), then the passage of electric current $\mathbf{j}$ causes the thermal flux $q_i = \pi_{ik} j_k$ to flow through a specimen (the Peltier effect).

Let us discuss the Seebeck effect. Direct action of the electric field and the temperature gradient on the electron subsystem gives rise to the drift $\mathbf{j}_{\text{drift}}$ and diffusion $\mathbf{j}_{\text{dif}}$ charge fluxes. The temperature gradient also produces the flow of phonons that move from the hot end of the specimen to the cold. Solely through the electron–phonon interaction (EPI), the phonons drag the charge carriers with themselves, thus increasing the thermoelectric current. This contribution into the current is j_{drag}. Observe that in this particular situation the total flux of charge carriers is zero: $\mathbf{j} = \mathbf{j}_{\text{drift}} + \mathbf{j}_{\text{drag}} + \mathbf{j}_{\text{dif}} = 0$ (Fig. 11).

In the case of standard semiconductors, the dimensions of the electron and the hole parts of Fermi surface are small compared with the radius of the Debye phonon sphere. Accordingly, when we talk about EPI, the laws of conservation of energy and momentum restrict from above the momentum p of phonons that can interact with charge carriers, namely, $p < 2k$, where k is the modulus of the electron wave vector. Thus, most of the phonons do not directly interact with the charge carriers. The 'electron phonons' can be scattered by charge carriers, whereas the rest are referred to as 'thermal phonons'. By definition, the electron phonons are long-wave, and therefore their relaxation times should be greater than those of thermal phonons. It is the nonequilibrium nature of such electron phonons (which is proportional to their relaxation times) that defines the magnitude of phonon-drag thermoelectric power.

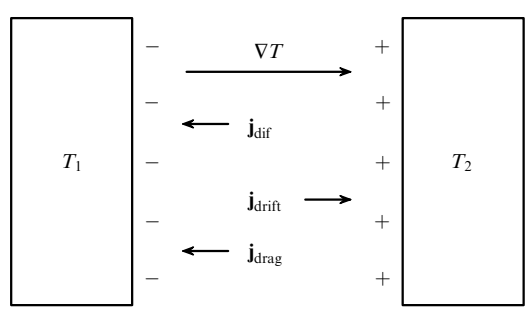

Figure 11. Charge fluxes in conductors that give rise to thermoelectric power.

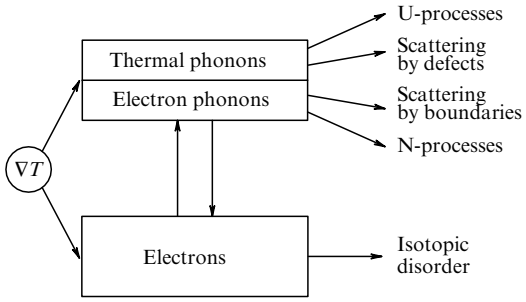

Figure 12. Scheme of the main processes of momentum relaxation in the system of electrons and phonons in the presence of temperature gradient.

Recall that even today there still are unresolved problems related to attenuation of long-wave phonons. In principle, the studies of thermoelectric power may throw some light on these issues.

Figure 12 depicts the scheme illustrating different scattering processes in the system of electrons and phonons, when there occurs a finite temperature gradient lengthwise of the sample. Such processes ensure both the relaxation of momentum received by the subsystems from the external field, and the redistribution of momentum between the subsystems. The main relaxation process for electrons is their scattering by impurities. For phonons, the following processes are important: scattering by the sample boundaries and point defects, and the Herring or Simons phonon–phonon scattering (these processes ensure relaxation of the total momentum of quasi-particles). At the same time, the electron–phonon scattering processes only result in the redistribution of momentum between electrons and phonons.

As indicated above, the current of charged particles is determined by the contributions from the drift and diffusion motion of electrons, and the contribution from the drag of electrons by phonons. Accordingly, thermoelectric power can be represented, generally speaking, as a sum of two terms: $Q = Q_{\text{dif}} + Q_{\text{drag}}$, where Q_{dif} is the diffusion thermoelectric power, and Q_{drag} is the phonon-drag thermoelectric power.

In the regime of impurity conduction, the diffusion thermoelectric power steadily increases with temperature, mainly because of the temperature dependence of chemical potential $\mu(T)$ (the system of charge carriers is described by the Boltzmann distribution, and therefore μ is several orders of magnitude greater than in metals). Phonon-drag thermoelectric power Q_{drag} prevails at low temperatures. Since the electrons only interact with the long-wave phonons, the temperature dependence $Q_{\text{drag}}(T)$ is determined by the interaction of these phonons with the boundaries of the specimen and with the short-wave phonons, to which they transfer their momentum. At very low temperatures, the main role for the electron phonons is played by the processes of their scattering by the boundary, and the redistribution of

momentum through EPI between the subsystems of quasiparticles is suppressed. A similar situation is observed at relatively high temperatures, when the intensity of anharmonic umklapp processes of the short-wave phonon interaction is increased. Broadly speaking, the maximum of $Q_{\rm drag}$ falls within the temperature range where the normal anharmonic processes prevail.

In the general case, the system of kinetic equations for electrons and phonons has not been solved. The results for certain particular cases are discussed in the monographs [9, 63 – 66].

Observe that Geballe and Hull [67] as early as 1954 discovered a considerable increase of thermoelectric power in germanium and the nonmonotonic behavior of $Q(T)$ at low temperatures. Shortly thereafter, C Herring constructed his theory of thermoelectric power in semiconductors [68] and interpreted the results reported in paper [67] as the effect of hole drag in germanium. We ought to emphasize, however, that Gurevich [69] was the first to demonstrate that the nonequilibrium phonon distribution at $\nabla T \neq 0$ at certain conditions may play an important role in thermoelectric phenomena. Of recent studies concerned with the effect of electron drag we point to Refs [70, 71] which report the temperature dependence $Q(T)$ in HgSe and HgSe:Fe crystals.

The effect of isotopic composition on thermoelectric power was the subject of just a few papers. Below we shall be mainly concerned with the experimental data. Then we discuss two possible scenarios for the dependence of Q on the isotopic disorder parameter ξ^2: the two-step electron – phonon drag, and the renormalization of anharmonic attenuation of long-wave phonons in the regime of weak localization.

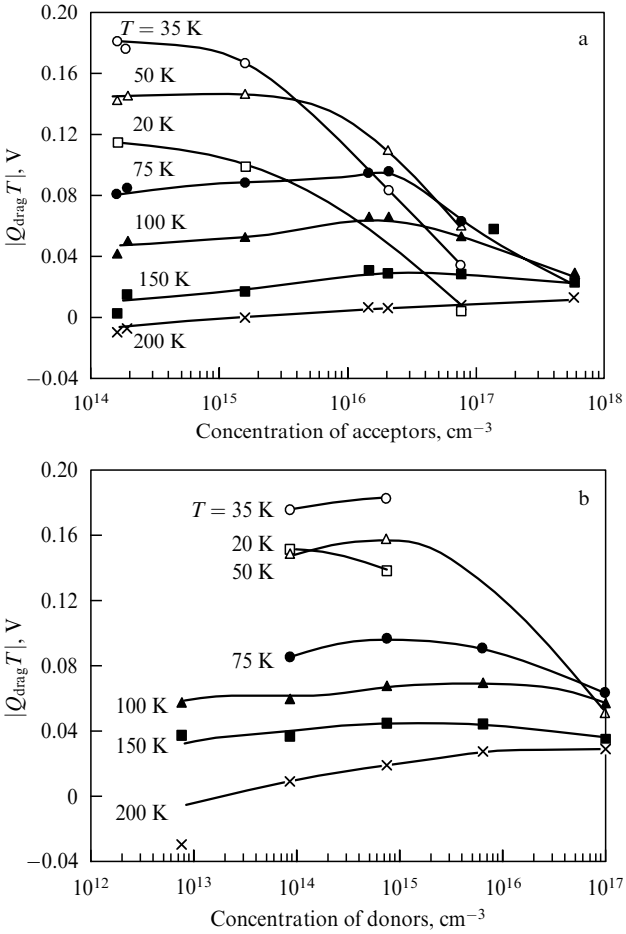

Figure 13. Dependence of the absolute value of the Peltier coefficient component due to the phonon drag for germanium single crystals of p type (a) and n type (b) on the concentration of acceptors and donors at different temperatures [67].

3.2 Germanium crystal thermopower

To the best of our knowledge, the effects of isotopic composition and isotopic disorder on thermoelectric power in crystals were studied so far in two papers [72, 73]. The temperature dependence $Q(T)$ was studied by Oskotskiĭ et al. [72] in tellurium specimens, one of which had the natural composition of isotopes, while the other was enriched with ^{128}Te to 92% and had the isotopic disorder parameter ξ^2 being smaller by the factor of 7.5 than that for the natural tellurium specimen. The isotopic composition was found to have no effect on the drag thermoelectric power over the temperature range from 4 to 50 K. The results of studying thermoelectric power of perfect germanium single crystals with three different isotopic compositions: natural, and highly enriched to 96.6% and 99.99% with ^{70}Ge were reported by Taldenkov et al. [73]. The specimens had the shape of a rectangular parallelepiped with the dimensions of about $0.25 \times 0.25 \times 4$ cm. The absolute measurements of thermoelectric power were carried out by the stationary temperature gradient method in the temperature range from 10 to 300 K.

It should be emphasized that for the studied germanium specimens of both p and n types, the difference of concentrations of donor and acceptor impurities was $|c_{\rm d} - c_{\rm a}| < 10^{14}\,{\rm cm}^{-3}$. With such low concentrations, as is well known [64, 67], the absolute magnitude of drag thermoelectric power exhibits practically no dependence on the number of electrically active impurities, and $|Q_{\rm drag}|$ at maximum must be close for the specimens of p and n types (Fig. 13). This allows us to compare data for all specimens under investigation, irrespective of the direction of the temperature gradient relative to crystallographic axes.

Experimental results in Fig. 14a for thermoelectric power $Q(T)$ were reproduced from Refs [73, 74]. They quite convincingly demonstrate the dependence of thermoelectric power on the measure of isotopic disorder ξ^2. The increase of $Q(T)$ with the decreasing ξ^2 occurs over the temperature range $T < 70$ K, where the thermoelectric power is mainly determined by the drag effect of charge carriers by phonons. At higher temperatures, when the diffusion component of thermoelectric power depending on the band parameters of the semiconductor dominates, the thermoelectric power is about the same for all the specimens.

Figure 14b shows the temperature dependence of the absolute value of the Peltier coefficient $\pi(T) = Q(T)T$ calculated from the experimental data on thermoelectric power for all specimens under investigation.The Peltier coefficient is directly seen to exhibit a strong dependence on ξ^2. To wit, as the concentration of ^{70}Ge isotope increases, the maximum of $|\pi(T)|$ increases too — that is, the drag effect becomes stronger.

3.3 Herring's drag thermopower

Let us consider a semiconductor with one type of carriers without degeneration and assume the presence of simple band structure. As already indicated, the electrons directly interact

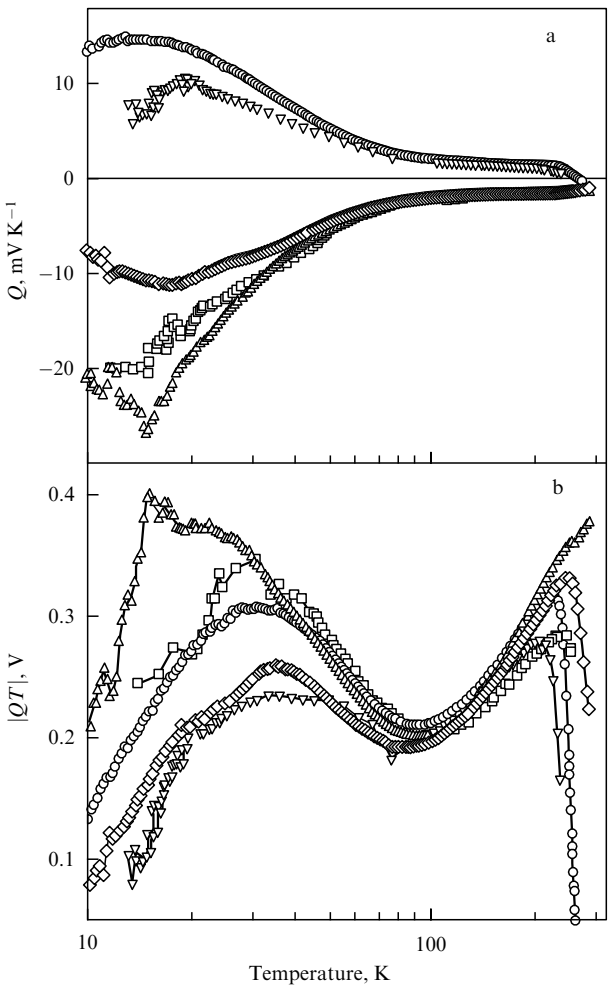

Figure 14. Temperature dependence of thermoelectric power (a) and absolute value of the Peltier coefficient (b) for germanium single crystals with different isotopic compositions [73, 74]: □ — ^{70}Ge(99.99 %) [100]; ○ — ^{70}Ge(96.3 %) [100]; Δ — ^{70}Ge(99.99 %) [111]; ▽ — ^{nat}Ge [100]; ◇ — ^{nat}Ge [111].

only with the long-wave phonons (electron phonons). Their effective relaxation times $\tau_{ph}(q)$, generally speaking, are much greater than those of thermal phonons. Accordingly, in the calculation of phonon-drag thermoelectric power in the first approximation the direct contribution from thermal phonons can be neglected: their drift velocity is assumed to be close to zero. The main scattering processes for the long-wave phonons are the anharmonic normal collisions with thermal phonons and the interaction with the sample boundary. The corresponding part of Q_{ph} is called the Herring's drag thermoelectric power, and denoted by $Q_{ph}^{(H)}$.

In the temperature range where the N-processes dominate, the Herring thermoelectric power is defined as

$$Q_{ph}^{(H)} = \frac{k_B}{e}\,\frac{m^* v_\circ^2}{k_B T}\,\frac{\widetilde{\tau}_{ph}}{\tau_{e-p}}\,, \tag{3.3}$$

where m^* and $v_\circ$ are the effective mass and the group velocity of an electron, respectively. We confine ourselves to considering the contribution from the longitudinal phonons, for which the mean relaxation time is given by

$$\widetilde{\tau}_{ph} = \frac{1}{4k^4}\int_0^{2k} \mathrm{d}q q^3 \tau_{ph}^{(N)}(q)\,, \tag{3.4}$$

where $\tau_{ph}^{(N)}(q)$ is the phonon relaxation time due to the anharmonic three-phonon N-processes, and τ_{e-p} is the relaxation time of electrons due to their interaction with phonons (see detailed discussion in Refs [64, 72]).

From expressions (3.3), (3.4) it follows that the behavior of phonon-drag thermoelectric power $Q_{ph}^{(H)}$ is determined by the dependence of $\tau_{ph}^{(N)}$ on the temperature and momentum: $\tau_{ph} \sim T^{5-j} q^j$. Observe that from the condition of convergence of the integral over $\mathrm{d}q$ emerges linkage with the problem of phonon attenuation. Namely, in the case of Pomeranchuk scenario [54], when $j = 4$, the thermoelectric power is $Q_{ph} = \infty$; in the case of Herring scenario [23], when the phonons interacting in the anharmonic manner have different polarizations and $j = 2$, the thermoelectric power Q_{ph} is finite. There also is the Simons scenario [24, 25], where $j = 1$ (in this case the attenuation of short-wave phonons is taken into account, which makes possible the processes of the type $l + l \rightleftharpoons l$, $t + t \rightleftharpoons t$).

Let us establish the relationship between the wave vector k from equation (3.3), which characterizes the upper limit of spectrum of electron phonons, and the Debye vector q_D. By definition, one has

$$k \simeq \frac{\sqrt{3 m_* k_B T}}{\hbar}\,, \quad q_D \simeq \frac{\pi}{a}\,. \tag{3.5}$$

In the case of germanium, the effective electron mass is $m_* \simeq 0.1m$. So $k \simeq 2 \times 10^5\, T^{1/2}$, and in the low-temperature range ($T \leqslant 50$ K) one finds

$$k \leqslant 10^{-2} q_D\,. \tag{3.6}$$

Now let us compare the mean free paths $L_A^{(N)}(l)$ as restricted by the anharmonic normal processes according to the Herring mechanism, with the mean free path L_{iso} determined by the standard isotope scattering. We use the results of studies concerned with germanium [44] [see relations (2.13)]. Then we have

$$L_A^{(N)}(l) \propto 10^{-1} \left(\frac{T_D}{T}\right)^3 \left(\frac{q_D}{q}\right)^2 a\,. \tag{3.7}$$

At temperatures $T \leqslant 20-30$ K, near the maximum of phonon-drag thermoelectric power, the following relation $L_A^{(N)}(l) \propto 10^3 (q_D/q)^2 a$ occurs for germanium. The mean free paths delimited by isotope scattering are

$$L_{iso} \propto \frac{1}{2\xi^2} \left(\frac{q_D}{q}\right)^4 a\,. \tag{3.8}$$

The concrete values of mean free paths L_{iso} for the specimens with natural isotopic composition and those enriched to 96.6% in ^{70}Ge to an order of magnitude are $10^3 (q_D/q)^4 a$ and $10^6 (q_D/q)^4 a$, respectively. From expressions (3.6)–(3.8) follow that the inequality $L_A^{(N)} \ll L_{iso}$ is fulfilled for mean free paths in the case of electron phonons, and in consequence the isotopic disorder in the standard theory has not to influence those part of the thermoelectric power that results from the Herring's drag.

Observe that to the left of the maximum the quantity $Q_{ph}^{(H)}(T)$ decreases with the temperature, as $\sim T^{-(9-j)/2}$, $j = 1, 2$. At the lowest temperatures, the main role belongs to the phonon scattering by the boundary of the specimen. In such a situation $Q_{ph}^{(H)} \sim d\, T^{3/2}$, where d is the characteristic diameter of the specimen (for details see Refs [64, 66]).

3.4 Two-step drag

In the analysis of the Herring type drag we assumed that the interaction with thermal phonons leads to the dissipation of momentum of the electron phonons. In reality, as has been first noted in Ref. [75] (see also paper [76]), the anharmonic interaction between the phonons (when the N-processes dominate) should give rise to a situation when the nonequilibrium thermal phonons drag the electron phonons, and the fluxes of phonons of the two groups flow with the same drift velocity. In such a case, the drag of charge carriers by phonons may occur in two stages: the carriers are dragged by the electron phonons, which in turn are dragged by thermal phonons.

In the situation of two-step phonon drag, the contribution to the thermoelectric power due to the nonequilibrium electron phonons is supplemented by the contribution from the nonequilibrium thermal phonons, which may be decisive. To an order of magnitude one has [75]

$$\widetilde{Q}T = (Q_1 + Q_2)T \sim \frac{\tau_{\rm ph}^{(\rm N)}(T) + \tau_{\rm ph}^{(\rm R)}(T)}{\tau_{\rm e-p}}\,. \tag{3.9}$$

Observe that in perfect single crystals the measure of departure from equilibrium for thermal phonons is determined by the relaxation time $\tau_{\rm ph}^{(\rm R)}(T)$ with respect to the anharmonic scattering umklapp processes. Thermoelectric power may then depend exponentially on the temperature. In semiconductors with isotopic disorder, the nonequilibrium character of thermal phonons must be suppressed through Rayleigh type scattering. Thus, the two-step phonon-drag thermoelectric power $\widetilde{Q}$, as opposed to the Herring type thermoelectric power $Q^{(\rm H)}$, depends on the measure of isotopic disorder ξ^2. It is interesting that with finite ξ^2 the dependence of $\widetilde{Q}$ on T is again a power function.

For germanium, it is possible to evaluate the mean free path $L_{\rm A}^{(\rm U)}(l)$ of longitudinal thermal phonons, delimited by the anharmonic scattering umklapp processes, using numerical parameters (2.13). It turns out then that

$$L_{\rm A}^{(\rm U)}(l) \propto 15\times 10^{-3}\left(\frac{q_{\rm D}}{q}\right)^2 \frac{330}{T}\exp\left(\frac{180}{T}\right) a \tag{3.10}$$

for thermal phonons ($q > 2k$). In the neighborhood of the maximum of $\widetilde{Q}$ at $T = 20(30)$ K we have

$$L_{\rm A}^{(\rm U)}(l) \propto 10^3(10^2)\left(\frac{q_{\rm D}}{q}\right)^2 a\,.$$

Now let us define the effective phonon mean free path $L_{\rm ph}^{(\rm R)}(T) = v_{\rm s}\tau_{\rm ph}^{(\rm R)}(T)$ as

$$\frac{1}{L} = v_{\rm s}\,\frac{\int {\rm d}\mathbf{q}\, C_q (v_q L_q)^{-1}}{\int {\rm d}\mathbf{q}\, C_q}\,, \quad C_q = \hbar\omega_q \frac{\partial}{\partial T} n_q\,. \tag{3.11}$$

Comparing $L_{\rm A}^{(\rm N)}(l)$ from Eqn (3.7) and $L_{\rm A}^{(\rm U)}(l)$ from Eqn (3.10), and getting an estimate for $L_{\rm ph}^{(\rm R)}(T)$, we find that to an order of magnitude $\tau_{\rm ph}^{(\rm N)}(T) > \tau_{\rm ph}^{(\rm R)}(T)$. This means that the contribution to $\widetilde{Q}$ from thermal phonons owing to the two-step drag is finite but not decisive.

In Ref. [76], the expressions for Q_1 and Q_2 are more rigorous than in Ref. [75], and the analysis of these expressions led to the conclusion that, in principle, the two-step phonon drag may dominate in the total thermoelectric power. Such a situation, however, is rather unlikely when the electron phonons are scattered through the Herring mechanism. If phonon scattering occurs through the Simons mechanism, then, according to Ref. [76], ''one may hope for the experimental discovery of drag effect in classical semiconductors''.

3.5 Weak localization regime

One of the mechanisms that may lead to the dependence of phonon thermoelectric power on the mass of isotopes is the specific anharmonic scattering mechanism studied in Ref. [77]. This paper discussed the influence of fluctuations of the phonon density in the regime of weak localization on the anharmonic interaction. Attenuation of long-wave phonons was evaluated with due account of the fact that a two-phonon coherent state arises in virtual states in the anharmonic diagrams. The analysis was performed in the general case in the approximation of diagonal disorder. It is shown that for $\{\omega, \mathbf{k}\} \to 0$ a significant contribution to the relevant mass operator is associated with the processes described by the diagram depicted in Fig. 15. Here γ_3 is the cubic anharmonic vertex. Thin line denotes the one-particle Green function G_k of the phonon mode with the quasi-momentum $\mathbf{k}$. Symbol U stands for the diffusion vertex. The latter occurs in the equation for the two-particle Green function and is defined by the set of standard fan-shaped diagrams (see the details in Ref. [77]).

The diagram presented in Fig. 15 corresponds to the analytical expression of the form

$$\Sigma_{\rm A}^{(i)}(\omega, \mathbf{k}) = {\rm i}\int_{-\infty}^{+\infty} {\rm d}\omega_1\, \frac{1}{1-\exp(-\beta\omega_1)} \times \sum_{\mathbf{q}\mathbf{q}_1} \Phi_{\mathbf{k},\mathbf{q}_1,-\mathbf{k}+\mathbf{q}_1}\, F(\omega,\omega_1;\mathbf{k},\mathbf{q}_1)\, \Phi^{(3)}_{\mathbf{k}-\mathbf{q}_1,\mathbf{q}_1,-\mathbf{k}}\,. \tag{3.12}$$

Here the notation was used:

$$F(\omega,\omega_1;\mathbf{k},\mathbf{q}_1) = \bar{G}^-_{-\mathbf{k}+\mathbf{q}_1}(\omega-\omega_1)\,\bar{G}^-_{\mathbf{q}_1}(\omega-\omega_1) \times U(q;\omega,\omega_1)\,\bar{G}^+_{-\mathbf{q}_1}(\omega_1)\,\bar{G}^+_{\mathbf{k}-\mathbf{q}_1}(\omega_1)\,, \tag{3.13}$$

where the Green function G_k is defined as

$$\bar{G}^-_k(\omega) = \left(\omega^2 - \omega_k^2 - {\rm i}\,\frac{\omega}{\tau_{\rm iso}(\omega)}\right)^{-1}, \tag{3.14}$$

and $\tau_{\rm iso}(\omega)$ is the phonon relaxation time due to the isotopic disorder.

We select the anharmonic vertex in the form

$$\Phi_{k_1k_2k_3} = -{\rm i}\widetilde{\gamma}_3\omega_{k_1}\omega_{k_2}\omega_{k_3}, \quad \widetilde{\gamma}_3 = \frac{\gamma^{(3)}}{\gamma'^{(2)3/2}}\,. \tag{3.15}$$

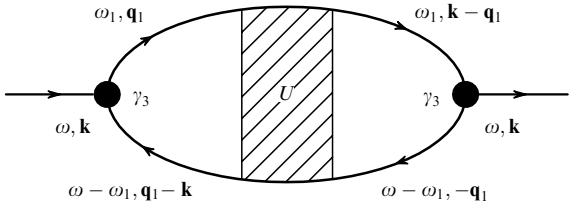

Figure 15. Anharmonic diagram with processes of coherent inverse phonon scattering in the weak localization regime.

For the diffusion vertex, in the fan approximation we arrive at the following chain of equalities:

$$U(q;\omega,\tilde{\omega}) = \left[1 - \frac{1}{N}\sum_{\mathbf{k}_1} \bar{G}^{+}_{\mathbf{k}_1}(\omega)\,\bar{G}^{-}_{\mathbf{k}_1-\mathbf{q}}(\omega-\tilde{\omega})\right]^{-1}$$

$$= \frac{\omega}{\pi\tau^2_{\mathrm{iso}}(\omega)}\,\frac{1}{g(\omega^2)}\,\frac{1}{D_0(\omega)\,q^2 - \mathrm{i}\tilde{\omega}}\,. \qquad (3.16)$$

Here, $D_0 = (1/3)v^2\tau_{\mathrm{iso}}$ is the diffusion coefficient, and v is the group velocity of the phonon mode.

Using relations (3.12), (3.14) and (3.16), we may demonstrate that the partial inverse relaxation time for the long-wave phonons ($\omega \ll \omega_{\mathrm{D}}$), which is due to the specific anharmonic processes, to an order of magnitude is determined by the relation

$$\tau_{\mathrm{A}}^{-1(i)} = \frac{\mathrm{Im}\Sigma^{(i)}_{\mathrm{A}}}{2\omega} \approx \xi^2\,\frac{\langle u^2\rangle}{a^2}\,\omega\,. \qquad (3.17)$$

For the mean free path we have

$$L^{(i)}_{\mathrm{A}} \propto \frac{1}{\pi\xi^2}\,\frac{a^2}{\langle u^2\rangle}\,\frac{q_{\mathrm{D}}}{q}\,a\,. \qquad (3.18)$$

Hence follows that the phonon free paths for germanium crystals with natural isotopic composition and with enrichment to 96% in ^{70}Ge are $10^6(q_{\mathrm{D}}/q)a$ and $10^9(q_{\mathrm{D}}/q)a$, respectively.

From comparison between relations (3.7) and (3.18) we find that for germanium crystals with natural isotopic composition the phonon free paths due to standard and specific anharmonic relaxation processes are of the same order of magnitude. Therefore, in such a situation the isotopic disorder may also indirectly affect the thermoelectric power.

Let us now summarize the above discussion. In the case of chemically pure single crystals of germanium with different isotopic compositions, the strong dependence of Q on the parameter ξ^2 was found experimentally in the temperature range dominated by the drag thermoelectric power. We discussed two mechanisms — the manifestation of elastic Rayleigh scattering processes in the two-step phonon drag, and the renormalization of the anharmonic phonon attenuation in the weak localization regime. These two mechanisms, broadly speaking, lead to the decrease of Q with increasing ξ^2. However, the specific mechanism of suppression of phonon-drag processes still awaits detailed theoretical analysis.

4. Isotope effects in the electric resistance of metals

Isotope effects in the phonon electric resistivity ρ of metals are mainly due to the change in the phonon spectrum brought on by the isotopic replacement of lattice atoms. In chemically pure substances, finite resistance also arises because of the static disturbances of the crystal lattice near isotopic impurities. In addition, the isotope effects, in principle, may influence the phonon-drag processes. It is usually assumed that the role of isotopes in the properties of the electron subsystem of metal (the shape of a Fermi surface, the dispersion law) ought to be secondary.

Observe that in the region of relatively high temperatures ($T \geqslant T_{\mathrm{D}}/3$) the resistance ceases to depend on the isotopic composition, because the electron–phonon interaction is quasi-elastic, and hence

$$\rho \propto \left\langle u^2(t=0)\right\rangle .$$

4.1 Effect of deformation of phonon spectrum because of the change of isotopic composition

Yu Kagan and one of the authors demonstrated in Ref. [78] that in the general case of monoatomic crystals with the mean atomic masses $M^{(1)}_{\mathrm{c}}$ and $M^{(2)}_{\mathrm{c}}$, the isotope effect in the phonon resistivity of metal is described by the universal relation of the form

$$\rho(M^{(1)}_{\mathrm{c}},T) = \rho(M^{(2)}_{\mathrm{c}},T')\sqrt{\frac{M^{(2)}_{\mathrm{c}}}{M^{(1)}_{\mathrm{c}}}}, \quad T' = T\sqrt{\frac{M^{(1)}_{\mathrm{c}}}{M^{(2)}_{\mathrm{c}}}}. \qquad (4.1)$$

Equation (4.1) was actually obtained for the monoatomic cubic crystals. As a matter of fact, this formula has a wider range of applicability and holds true for crystals with arbitrary symmetry. This circumstance is related to the fact that the polarization vectors in monoatomic crystals, unlike the phonon frequencies, do not depend on the atomic mass (see Appendix B). The expression of the type (4.1) is valid for the individual components of the electric conductivity tensor reduced to the major axes. Relation (4.1) is also found in the context of Bloch–Grüneisen theory, according to which (see, for example, book [9])

$$\rho(M,T) = 4\left(\frac{T}{T_{\mathrm{D}}}\right)^5 J_5\left(\frac{T}{T_{\mathrm{D}}}\right)\rho(T_{\mathrm{D}})\,, \qquad (4.2a)$$

$$J_n\left(\frac{T}{T_{\mathrm{D}}}\right) = \int_0^{T_{\mathrm{D}}/T} \frac{z^n\,\mathrm{d}z}{(e^z-1)[1-\exp(-z)]}\,. \qquad (4.2b)$$

Here, the parameter $\rho(T_{\mathrm{D}})$ is the resistivity in the classical limit at $T = T_{\mathrm{D}}$, and $\rho(T_{\mathrm{D}}) \propto MT_{\mathrm{D}}^{-2}$. In the low-temperature range, when ρ obeys Bloch's law, from Eqns (4.1), (4.2) it follows that $\rho \propto M^2T^5$. So that the isotope effect in the resistance is described by the relation

$$\frac{\rho(M^{(2)}_{\mathrm{c}},T) - \rho(M^{(1)}_{\mathrm{c}},T)}{\rho(M^{(1)}_{\mathrm{c}},T)} \approx 2\,\frac{M^{(2)}_{\mathrm{c}} - M^{(1)}_{\mathrm{c}}}{M^{(1)}_{\mathrm{c}}}\,. \qquad (4.3)$$

In this way, the change in the phonon spectrum owing to the isotopic substitution leads to the linear effect with respect to the mass difference at low temperatures. It is interesting that the resistance in the case of a heavy isotope is higher than in the case of a light isotope. Generally speaking, the isotope effect may be as large as 10%. At higher temperatures, as indicated above, the resistance ceases to depend on the mass of the lattice atoms, and hence on the isotopic composition.

It should be emphasized that the main contribution to the resistivity $\rho(T)$ of simple metals with the one-sheet Fermi surface (alkali metals, aluminium) comes from the electron scattering umklapp processes (U-processes). At low temperatures, when the long-wave phonons are only excited, the umklapp transitions are only possible for the electrons located on the isolated 'hot spots' of the Fermi surface (i.e. in the domains where the electron relaxation rate is at a maximum). Such transitions occur with the participation of phonons with a certain characteristic frequency $\omega^*_{\mathrm{ph}}(\mathbf{q}_{\min})$ (Fig. 16). In such a situation, the resistivity may vary according to the exponential law: $\rho(T) \sim \exp(-\hbar\omega^*_{\mathrm{ph}}/k_{\mathrm{B}}T)$,

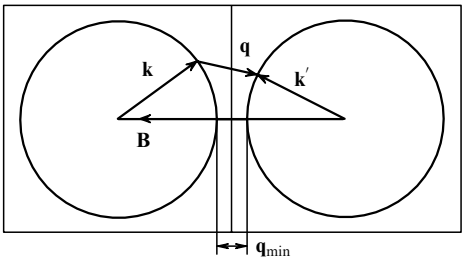

Figure 16. Electron – phonon umklapp processes in the scheme of repeating bands.

and the effect of deformation of the phonon spectrum brought on by the isotopes must be heightened.

Observe that in the case of electric conductivity the fine structure of the nonequilibrium electron distribution function is determined by the anisotropy of the electron – phonon interaction due to the umklapp processes. The anisotropy of the phonon spectrum sharpens the singularities of the distribution function.

For most metals, the Fermi surface consists of many sheets and is very complicated. Division of the electron – phonon processes into the normal processes and umklapp processes does not cover the entire diversity of possibilities. We must also consider the scattering processes in which the nonequilibrium electrons either stay on the same sheet of the Fermi surface or move from one sheet to another. Such processes are usually referred to as, respectively, intrasheet and intersheet processes. Notice that the intersheet processes give rise to a specific anisotropy of electron – phonon interaction, caused by the local peculiarities of the Fermi surface topology.

There are several types of peculiarities innate to the Fermi surface: (1) regions of closest approach of the sheets in fixed directions, so that the gap between the sheets remains finite (gap case), and (2) conical points of contact of sheets (zero-gap case). Such points occur for those parts of the Fermi surface where the spin – orbit interaction owing to a crystal symmetry does not remove the degeneration in the electron spectrum. All metals with the HCP (hexagonal close packing) structure necessarily exhibit degeneracy. Peculiar features of the electron spectrum also include thin bridges, very small split-off cavities, narrow layers of open trajectories (see details in monograph [79]). For the electron – phonon intersheet transitions the law of conservation of momentum is expressed as follows: $\mathbf{k}_2 = \mathbf{k}_1 + \mathbf{q} + \mathbf{Q}_{12}$, where $\mathbf{Q}_{12}$ is the distance between the centers of the sheets 1 and 2. In the region of approach of the sheets the electron may be efficiently scattered to large angles at relatively low temperatures. Such processes freeze out at such T for which the momentum of acoustic phonons with the frequency $\omega(\mathbf{q}) \leqslant k_B T/\hbar$ satisfies the condition $q \leqslant \delta k$ (where δk is the gap width). Accordingly, we may speak again of hot spots, this time, however, on separate sheets. In such a situation the effect of isotopes may once again be more pronounced than it would follow from formula (4.3).

The results of just a few experimental studies concerned with the isotope effects in the resistance of metals have been published. In the earlier works, the linear isotope effect was studied with lithium [80 – 82] and cadmium samples [83]. Figure 17 depicts the temperature dependence of the resistance of lithium isotopes, and Fig. 18 illustrates the

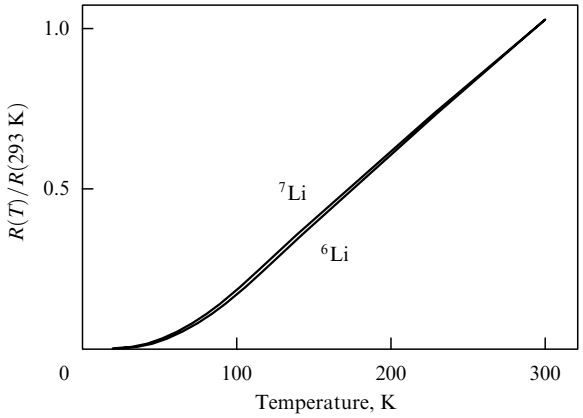

Figure 17. Experimental temperature dependences of electric resistance of ^{6}Li and ^{7}Li isotopes [82]. Typical dimensions of the specimen are: $L = 25$ cm, $\varnothing = 1$ mm, RRR (^{6}Li) ≈ 590, RRR (^{7}Li) ≈ 730.

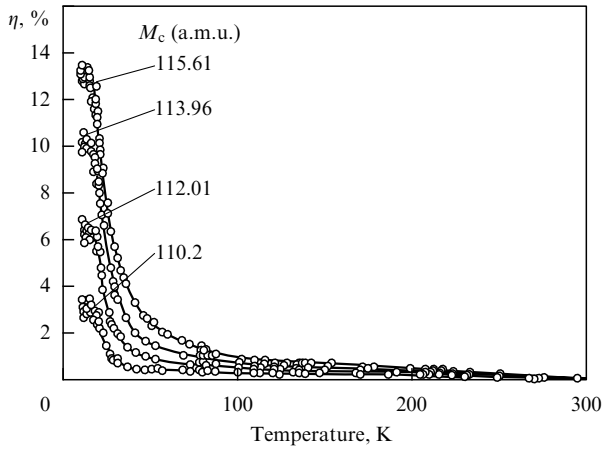

Figure 18. Temperature dependence of the relative change of electric resistivity of cadmium samples with different isotopic compositions; $\eta = [\rho_i(T) - \rho_i(0)]/[\rho_1(T) - \rho_1(0)] - 1$, where ρ_i is the resistivity of the specimen with a given isotopic composition, normalized to its resistivity at $T = 291$ K; ρ_1 is the same for the specimen with the least isotopic mass $M_c = 108.2$ a.m.u. [83]. Typical dimensions of the specimen are: $L = 60$ cm, $\varnothing = 0.65$ mm, RRR $\approx 300 - 400$.

relative variation of the resistance of cadmium isotopes. The results of these experimental studies agree well with the theory at temperatures above about 20 K, where chemical impurities have little effect on the temperature dependence of the resistance.

Accurate measurements of the resistance of lithium isotopes ^{6}Li, ^{7}Li, and the isotopic alloy $^{7+6}$Li at low temperatures, carried out in Ref. [84], allowed separation of the effects caused by chemical impurities from the isotope effects. Observe that isotopic substitution leads to the deformation of phonon spectrum, which, as demonstrated above, changes the temperature dependence of electric resistivity at low temperatures (Fig. 19). Chemical impurities, in turn, create static disordering in the lattice. Elastic phonon scattering by point defects in lithium, whose Fermi surface is nearly spherical, may be approximately regarded as isotropic. Accordingly, for $T \ll T_D$ the impurities suppress the fine structure of the nonequilibrium part of the electron distribution function $\delta f_{\mathbf{k}}$, characteristic of a perfect crystal, which originally arises because of the anisotropic inelastic

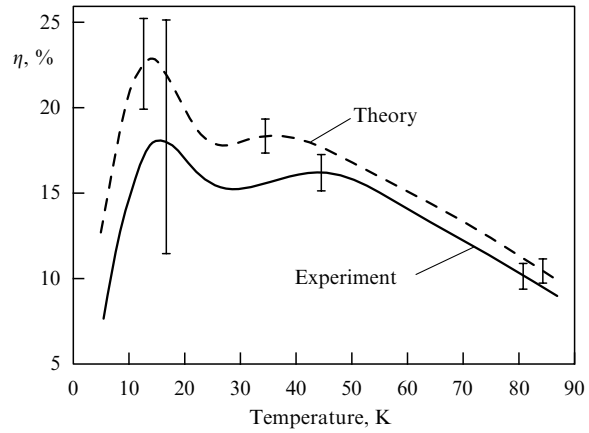

Figure 19. Temperature dependence of the isotope effect on electric resistivity for 'pure' lithium specimens with ^{6}Li and ^{7}Li isotopes; $\eta_{\Delta M} = ({}^7\rho - {}^6\rho)/{}^6\rho$ [84].

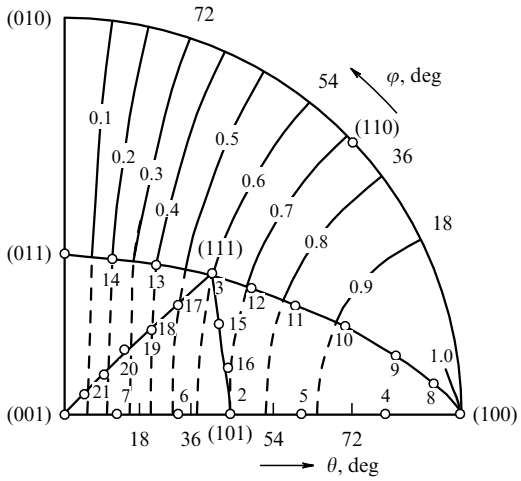

Figure 20. Stereographic projections of the curves $k_x = \text{const}$; points are the nodes of the quadrature grid for the irreducible part of the Brillouin zone [86].

scattering umklapp processes. The dependence $\rho(T)$ is also altered as a result of this impact (see, for example, the review by Bass [85]). Observe that for lithium both these effects must have an important bearing on the dependence of ρ on T.

Figures 20 and 21 show theoretical data on the change in the nonequilibrium part of the electron distribution function $\delta f_{\mathbf{k}}$ on the Fermi surface (FS) in a regular crystal. The trivial dependence $\delta f_{\mathbf{k}} \sim k_\alpha$ is illustrated in Fig. 20. The nontrivial dependence of $\delta f_{\mathbf{k}}$ on $\mathbf{k}_F$ is described by the function of the type

$$\delta g_\alpha(\mathbf{k}_F) = \frac{\delta f_\alpha(\mathbf{k}_F)}{c_1^\alpha} - k_F^\alpha .$$

Stereographic projections of the curves $\delta g_\alpha(\mathbf{k}_F) = \text{const}$ for three values of the temperature are depicted in Fig. 21. 'Hot spots' on FS occur in the region near the point (110). As follows from the diagram corresponding to the temperature $T/T_D = 0.05$ at which the umklapp processes freeze out, the value of δg_α is the lowest at $\mathbf{k}_F \in (110)$. The nonequilibrium electrons 'leave' that region of FS where they are scattered most efficiently. At temperatures $T/T_D = 0.02$ and $T/T_D = 0.2$, which are lower and higher than $T/T_D = 0.05$, the role of U-processes in the electric resistance is less important. Accordingly, the value of δg_α at $\mathbf{k}_F \in (110)$ is less (in magnitude).

Four groups of lithium specimens with varying degree of chemical purity: ^{6}Li (ratio of the resistance at room temperature to the residual resistance RRR = 800), ^{7}Li (RRR = 1000), ^{7}Li (RRR = 370), and the alloy of isotopes $^{7+6}$Li (44.5% ^{6}Li and 55.5% ^{7}Li, RRR = 650) were studied in Ref. [84]. The specimens were prepared in the form of a wire approximately 30 cm in length and 0.5 mm in diameter. The resistivity was measured by the standard four-probe method using direct current. The experimental data for the isotope effect $\eta_{\Delta M} = ({}^7\rho - {}^6\rho)/{}^6\rho$ in the most chemically pure specimens (RRR = 1000) are depicted in Fig. 19 with the solid line. The dashed line in the same diagram shows theoretical results obtained from the universal relation

$${}^7\rho(T) = {}^6\rho(T')\sqrt{\frac{{}^6M}{{}^7M}},$$

where $T' = T\sqrt{{}^7M/{}^6M}$. We notice that theoretical and experimental curves lie close to each other.

Figure 22 shows the curves for specimens with a relatively high content of chemical impurities. In this case the experimental curves *2* and *3*, which describe the isotope effect on ρ in the mixture of isotopes:

$$\eta' = \frac{{}^{7+6}\rho - {}^6\rho}{{}^6\rho}, \tag{4.4a}$$

$$\eta'' = \frac{{}^7\rho - {}^{7+6}\rho}{{}^7\rho}, \tag{4.4b}$$

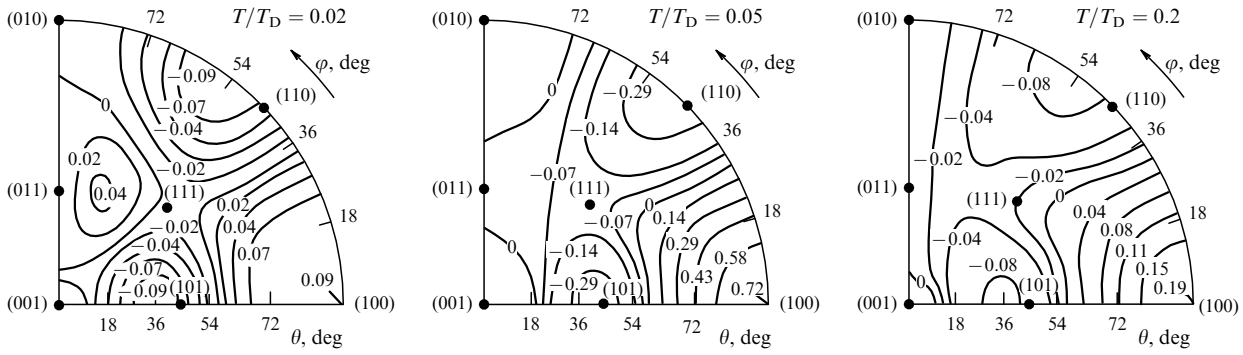

Figure 21. Angular structure of the nonequilibrium electron distribution $g(\mathbf{k}_F)$ for lithium.

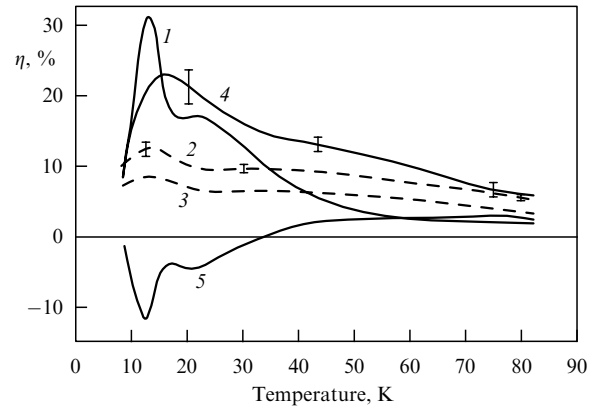

Figure 22. Temperature dependence of the change in electric resistivity $\eta(T)$ of lithium caused by the isotope effect and the phenomenon of isotropization. Solid curves are plotted from experiments, and dashed from calculations: *1* — $\eta_{\rm im} = ({}^{7}\rho_{\rm im} - {}^{7}\rho)/{}^{7}\rho$, *2* — $\eta'_{\Delta M,\,\rm theor} = ({}^{7+6}\rho - {}^{6}\rho)/{}^{6}\rho$, *3* — $\eta''_{\Delta M,\,\rm theor} = ({}^{7}\rho - {}^{7+6}\rho)/{}^{7}\rho$, *4* — $\eta' = ({}^{7+6}\rho - {}^{6}\rho)/{}^{6}\rho = \eta'_{\Delta M} + \eta'_{\rm im}$, *5* — $\eta'' = ({}^{7}\rho - {}^{7+6}\rho)/{}^{7}\rho = \eta''_{\Delta M} + \eta''_{\rm im}$ [84].

do not fit in with the theoretical curves *4* and *5* calculated from the universal relation. The reason is that a $^{7+6}$Li specimen differed from ^{7}Li and ^{6}Li ones not only in the isotopic composition but also in chemical purity: the $^{7+6}$Li specimen was less chemically pure than the ^{7}Li and ^{6}Li specimens. The influence of $\delta f_{\mathbf{k}}$ isotropization with foreign impurities on the resistivity $\rho(T)$ is described by the parameter $\eta_{\rm im} = ({}^{7}\rho_{\rm im} - {}^{7}\rho)/{}^{7}\rho$ which defines the relative difference in the resistivities of 'dirty' and 'pure' ^{7}Li specimens. The corresponding curve in Fig. 22 is marked with the number *1*. Taking the impurities into account, in place of expressions (4.4) we get

$$\eta' = \eta'_{\Delta M} + \eta'_{\rm im}\,, \tag{4.5a}$$

$$\eta'' = \eta'_{\Delta M} - \eta'_{\rm im}\,. \tag{4.5b}$$

In other words, curves *4* and *5* can be represented as the sum and the difference of the curve *1* and curves *2* and *3*.

In this way, the isotopic lithium alloys were employed for observing a significant change in $\rho(T)$ caused both by the isotopic deformation of the phonon spectrum and by the partial suppression of the fine structure of the nonequilibrium part of the electron distribution function $\delta f_{\mathbf{k}}$ owing to the phonon elastic scattering by foreign chemical impurities.

4.2 Residual resistivity

Now let us discuss the issue of the residual electric resistance of chemically pure metals comprising the mixtures of isotopes. For qualitative approach, we assume that the electron Fermi surface is nearly spherical. Then for the description of the residual resistivity we can use the expression of the form (see, for example, book [9])

$$\rho_{\rm r} = \frac{m}{ne^2}\,\frac{1}{\tau_{\rm iso}}\,,\quad \frac{1}{\tau_{\rm iso}} = \frac{mk_{\rm F}}{\pi\hbar^3\Omega_0}\int_0^1 {\rm d}\left(\frac{q}{2k_{\rm F}}\right)\left(\frac{q}{2k_{\rm F}}\right)^3 S(\mathbf{q})\,. \tag{4.6}$$

Here we used the following notation: e and m are the elementary charge and the electron mass, n is the electron density, $\mathbf{q}$ is the scattering vector, and $\mathbf{k}_{\rm F}$ is the electron momentum on the Fermi surface. Also, the factor $S(\mathbf{q})$ that characterizes the elastic Born scattering of electrons in the lattice with a dynamic and static disorder is defined as

$$S(\mathbf{q}) = \frac{1}{N}\sum_{\mathbf{nn}'} \exp\left[{\rm i}\mathbf{q}(\mathbf{R}_{\mathbf{n}} - \mathbf{R}_{\mathbf{n}'})\right] V_{\mathbf{n}}(\mathbf{q}) V_{\mathbf{n}'}(\mathbf{q})\,, \tag{4.7a}$$

where $\mathbf{R}_{\mathbf{n}} = \mathbf{R}^{(0)}_{\mathbf{n}} + \boldsymbol{\zeta}_{\mathbf{n}}$, and $V_{\mathbf{n}}(\mathbf{q})$ is the Fourier component of the electron–ion pseudopotential.

The pseudopotential $V_{\mathbf{n}}$, which describes the electron scattering from the **n**th ion, is the product of the static part V_0, whose value does not change from one lattice site to another, and the dynamic Debye–Waller (DW) factor $W_{\mathbf{n}}(\mathbf{q}) = \langle(\mathbf{q}\mathbf{u}_{\mathbf{n}}(0))^2\rangle$ depending on the mass of the vibrating atom:

$$V_{\mathbf{n}}(\mathbf{q}) = V_0(\mathbf{q}) \exp\left[-\frac{W_{\mathbf{n}}(\mathbf{q})}{2}\right], \tag{4.7b}$$

so that the difference $V_{\mathbf{n}} - V_{\mathbf{n}'}$ is nonzero and leads to a finite resistivity together with the field of static displacements.

Since the dynamic and static displacements are small compared with the interatomic spacing, we may expand the exponents in formulas (4.7) and keep only the first three terms. The terms that contain delta-function with respect to momentum do not give rise to electric resistance. Accordingly, the scattering of the conduction electrons is described by the expression of the form [87]

$$S(\mathbf{q}) \approx \frac{1}{N}\left\{\frac{1}{2}\,\Delta W(\mathbf{q})\,\Delta W(\mathbf{q}) + \left(\mathbf{q}\boldsymbol{\zeta}\,(\mathbf{q})\right)\left(\mathbf{q}\boldsymbol{\zeta}\,(\mathbf{q})\right) + \left[\left(\mathbf{q}\boldsymbol{\zeta}\,(\mathbf{q})\right)\Delta W(\mathbf{q}) - \left(\mathbf{q}\boldsymbol{\zeta}^{\,*}(\mathbf{q})\right)\Delta W(\mathbf{q})\right]\right\}. \tag{4.8}$$

The explicit expression for the spatial Fourier component of static displacements $\boldsymbol{\zeta}(\mathbf{q})$ was obtained in the review [88, see Section 3]. As far as the dynamic factor is concerned, in the ideal lattice $W_{\mathbf{n}}$ does not depend on the nodal index **n**. Because of this, it is the Fourier component of the quantity $\Delta W_{\mathbf{n}} = W_{\mathbf{n}}(\Delta M \neq 0) - W_0(\Delta M = 0)$ that occurs in Eqn (4.8). We have then

$$\begin{aligned}\Delta W(\mathbf{q}) &= \frac{1}{N}\sum_{\mathbf{n}} \exp\left[{\rm i}\mathbf{q}\mathbf{R}^{(0)}_{n}\right]\Delta W_{\mathbf{n}} \\ &= \frac{1}{N}\sum_{\mathbf{n}} \exp\left[{\rm i}\mathbf{q}\mathbf{R}^{(0)}_{\mathbf{n}}\right] q^{\alpha} q^{\beta}\,\Delta K^{\alpha\beta}_{\mathbf{nn}} \\ &= -\frac{1}{2} q_{\alpha} q_{\beta}\,\frac{\Delta M}{M_0}\sum_{\mathbf{q}_1 j_1 j_2} Z^{\alpha\beta}_{\mathbf{q}_1 j_1,\,\mathbf{q}+\mathbf{q}_1 j_2}\,.\end{aligned} \tag{4.9}$$

From the arguments put forward above it follows that the first term in formula (4.8) describes scattering due to the difference between the dynamic Debye–Waller factors of the matrix atom and the isotopic impurity, the second term describes scattering by near-impurity static displacements, and the third term bears the responsibility for the interference scattering.

If the impurities are regarded as isolated, then in the calculation of resistivity the quantity $1/N$ in Eqn (4.8) must be replaced with the defect concentration c. In the case of isotopic mixture in place of c we have the isotopic disorder parameter ξ^2.

We use the simplest model of the linear atomic chain (see relations (3.15) and (3.16) from Section 3 of the review [88])

and evaluate the quantities $\Delta W(q)$ and $q\zeta(q)$. Relying on expression (4.9) and Eqn (3.13) from Ref. [88], we may show, in the first place, that

$$\Delta W(q) \propto -\frac{1}{2}\,\epsilon q^2 l^2\,. \tag{4.10}$$

At the same time, using Eqns (3.13a) – (3.13d) from the review [88], we get

$$q\zeta(q) \propto -\frac{1}{2}\,\lambda\epsilon\,\frac{\sqrt{f_2/M_0}}{\omega_q}\,ql\,,\quad \lambda=\frac{g_3 l}{2f_2}>1\,. \tag{4.11}$$

Hence it follows that in the region of small and intermediate values of the scattering vector $\mathbf{q}$, where the potential $V_{\mathbf{n}}(\mathbf{q})$ is not small, it is the phonon scattering caused by static deformation of the lattice that dominates. In the range of q close to $2k_{\mathrm{F}}$ (i.e. at large scattering angles), when $V_{\mathbf{n}}(2k_{\mathrm{F}}) \ll V_{\mathbf{n}}(q=0)$, the contribution from scattering caused by the difference of the dynamic factors $W_{\mathbf{n}}$ may be important as well.

In the framework of the microscopic theory of kinetic coefficients relating to regular metals [89], the calculations of residual resistivity for lithium, which has two stable isotopes ^{6}Li and ^{7}Li, were carried out in Ref. [87]. It was estimated that the contributions to ρ_{r}, associated with the difference in the dynamic amplitudes of the electron – ion interaction and with the fields of the static displacements near impurities, differ approximately by a factor of five. The contribution caused by a lattice distortion here dominates.

Notice that in weak metallic solutions with the standard substitution impurities the residual resistivity is determined via the processes of electron scattering by the defects, which result from the difference of static amplitudes. The contribution to ρ_{r} owing to phonon scattering by matrix atoms displaced near a defect is relatively small. The exception are the isoelectronic weak solutions, where the inclusion of lattice distortion into consideration may change ρ_{r} by several tens of percent (see, for example, Ref. [90]). It is only in the case of chemically pure metals with isotopic impurities that scattering processes related to static displacements may prevail.

Isotopic disorder in the lattice restricts the mean free path of the conduction electrons. It is well knows that in the nontransition metals at room temperature the free path is determined by electron scattering from phonons, and (see, for example, book [9]) $\Lambda_{\mathrm{ph}} \sim 50\,T_{\mathrm{m}}/T$, where T_{m} is the melting point. The value of Λ_{ph} is several hundred angstroms. At absolute zero temperature, in a metal with isotopic disorder the mean free path Λ_{iso} associated with scattering caused by the difference of dynamic amplitudes and static displacements, to an order of magnitude is given by

$$\Lambda_{\mathrm{iso}} \sim \frac{1}{\xi^2}\,\frac{l^2}{\langle u^2\rangle}\,\frac{1}{\Upsilon}\left(\frac{V_0(2k_{\mathrm{F}})}{V_0(q=0)}\right)^2\Lambda_{\mathrm{ph}}\,, \tag{4.12}$$

where Υ takes care of the resistance increase because of static displacements. To an order of magnitude, the estimate $\langle u^2\rangle/l^2 \sim 10^{-3}$ is valid. In the case of natural isotopic mixtures of such metals as lithium, zinc and tin, we have $\xi^2 \geqslant 10^{-4}$. For molybdenum, $\xi^2 \approx 6\times10^{-4}$. For these metals $\Lambda_{\mathrm{iso}} \sim 0.1$ cm, and disregarding the distortion ($\Upsilon=1$) — $\Lambda_{\mathrm{iso}} \sim 1$ cm. Estimates show that in the case of strongly disordered isotopic mixtures — for example, mixtures of equal amounts of two isotopes — the mean free paths Λ_{iso} may decrease more than tenfold owing to the increase in the isotopic disorder parameter ξ^2.

I Pomeranchuk was the first to point out in paper [91] that chemically pure metals, which contain different isotopes at lattice points, at zero temperature will exhibit finite residual resistivity ρ_{r} because of the dynamic disorder. According to his theory, the resistance arises in a higher order with respect to the electron – ion interaction than in the Born approximation. The isotope effect is due to the fact that the phonons arising in virtual states in the scattering of electrons experience the influence of isotopic disorder. The resistivity ρ'_{r} corresponding to this process is proportional to the parameter of the electron – ion interaction to the fourth power. As compared with Eqn (4.6), the expression for ρ'_{r} contains an additional term $[V_0(2k_{\mathrm{F}})/\epsilon_{\mathrm{F}}]^2$ (where ϵ_{F} is the Fermi energy) which for the normal metals is very small (see, for example, Ref. [92]). Because of this, the contribution to the electric resistance due to the process proposed by Pomeranchuk [91] is apparently insignificant.

Kagan and one of the authors demonstrated in Ref. [78] that a finite resistivity ρ_{r} in the lattice with isotopic disorder exists already in the Born approximation. Namely, the true pseudopotential $a_{\mathbf{n}}$ of electron scattering by $\mathbf{n}$th ion is the product of the static part V_0 and the Debye – Waller factor. As a result, the difference $V_{\mathbf{n}} - V_{\mathbf{n}'}$ is nonzero, and the residual resistivity appears already in the standard approximation. The effects on ρ_{r} of the fields of static displacements $\{\zeta_{\mathbf{n}}\}$, which arise near the isotopic impurities, was analyzed in Ref. [87]. The contribution related to the difference in the dynamic factors was also taken into account.

To the best of our knowledge, the problem of residual electric resistance in isotopically inhomogeneous metal has previously been studied experimentally only by Zernov and Sharvin [93] with tin of natural isotopic composition. Measurements of the resistance of several single-crystal tin specimens of varying degree of purity were performed with contactless method based on measuring the moment of forces acting on the spherical specimen in rotating magnetic field. The diameter of the tin spheres was about 12.6 mm. The mean free path of the electrons at $T \to 0$, which was about 3 mm in the purest of all the specimens, may be restricted by scattering from isotopes, because the theory [87] predicts the value of 1 to 10 mm. Detailed comparison with the theory requires measurement data for specimens with different isotopic compositions.

5. Conclusions

In the past decade, interesting and important results have been obtained in the study of the effects of isotopic disorder on the kinetic coefficients. In the first place we should mention the studies of thermal conductivity $\varkappa(T)$, where the influence of isotopic disordering of the crystal lattice is the strongest. The experiments have been performed with perfect single crystals of carbon, germanium, and silicon with different isotopic compositions, including highly enriched crystals, in a wide temperature range. It was found that at room temperature the phonon scattering from the fluctuations of isotopic mass restricts considerably the thermal conductivity in crystals with natural isotopic composition. For germanium and silicon, the change of $\varkappa(T)$ at the maximum at low temperatures depending on the measure of isotopic disorder ξ^2 was studied. As far as the theory of lattice thermal conductivity is concerned, the phenomenological Callaway model which takes into account the anharmonic N- and U-processes has been extended to the case of systems

with strongly anisotropic phonon spectrum. This model has been used for studying the role of different processes of phonon scattering. Thermal conductivity of germanium and silicon was also considered in the context of microscopic approach based on the straightforward solution of the kinetic equation. A significant contribution from optical modes to heat transfer was discovered. The fine structure of the nonequilibrium phonon distribution function is also important here.

Theoretical calculations performed so far permit us to describe the effects of isotopic disorder on the behavior of $\varkappa(T)$ both at the maximum and at room temperature only at the qualitative level. Considerable quantitative discrepancy between the theory and experiment calls for more advanced theoretical treatment, and in particular the study of the role of anisotropy in elastic phonon scattering by isotopes.

Along with the heat transfer, where the isotopic disordering may lower the thermal conductivity by as much as an order of magnitude at low temperatures, studies have begun of the isotope effects on thermoelectric power $Q(T)$ in semiconductors. In the case of low temperatures, where the main contribution to thermoelectric power comes from the electron drag by long-wave phonons, the Rayleigh type scattering processes ($\sim \omega^4$) are not efficient for these phonons, and the quantity $Q(T)$ should not depend on the measure of isotopic disorder ξ^2. The experiment revealed, however, that in germanium crystals the magnitude of thermoelectric power decreases considerably as ξ^2 increases. Such a behavior may be attributed to the suppression of the two-step drag processes because of the isotopic disorder. Other scenarios are also possible — for example, the manifestation of weak localization processes in the anharmonic phonon gas. As yet, there is no detailed theoretical treatment of the results of this experiment, based on the microscopic models for germanium. Observe that theoretical analysis ought to be performed with due account for the anisotropy of the phonon spectrum and inclusion of two groups of phonons (*l*- and *t*-modes). Also, the availability for charge carriers of the electron and hole sheets of the Fermi surface must be explicitly taken into account. The interference between elastic and inelastic scattering processes which considerably modify the steady distributions of electrons and phonons may also be important. Note that in this case it is also necessary to take into consideration the elastic scattering of electrons from static displacements which arise in crystals with several different isotopes.

The isotope effects in the electric resistivity $\rho(T)$ of metals are generally small. Observation of the linear (with respect to the isotope mass difference) effect due to the distortion of the phonon spectrum under changes of the isotopic composition is hindered by foreign impurity atoms which initiate the suppression of the fine structure of the nonequilibrium electron distribution function. As far as the effects of the second order are concerned, they lead to a finite electric resistivity ρ_r for $T \to 0$. According to theoretical evaluations, elastic scattering of electrons by static displacements near the isotopes in chemically pure compounds may determine the magnitude of the resistivity ρ_r.

Modification of properties of single crystals, like changing their thermal conductivity, by controlling the proportion of isotopes is becoming a useful method in the production of materials for various applications. For example, the isotopically enriched diamond proved to be a much better monochromator of synchrotron radiation than natural diamond [94]. A dramatic increase in the thermal conductivity of isotopically enriched silicon, declared by Ruf and colleagues [48], prompted an attempt to put this material to commercial use in microelectronics (see the appropriate information on the site of ISONICS company at http://www.isonics.com).

New high-precision data have been published in the past 10 or 15 years on the effects of isotopic composition of semiconductors on their structural properties and electron spectrum. This discussion, however, goes beyond the scope of our review. Let us just remark that the review of first (mainly experimental) data concerning isotope effects on structural properties of solids was done by V S Kagan in 1962 [95]. Isotopic effects on the electron spectrum of semiconductors are discussed in Refs [96 – 100].

In conclusion, let us make a few general remarks. From theoretical standpoint, the study of isotope effects in solids is a highly intriguing task. In most cases the change of the isotopic mass is a small parameter of the theory, which gives the opportunity of performing a consistent analytical renormalization of a given physical quantity in the form of a functional of the spectral characteristics of the regular crystal. This allows one to make detailed calculations based on the tested microscopic models with the known values of parameters. Oftentimes, the isotopic shifts of concrete physical quantities are determined by more or less equal contributions from different effects. This calls for special care in the calculations. It ought to be mentioned also that the study of isotope effects resulting from isotope substitution is often a good touchstone for more general theories and theoretical models.

As for the experiments concerned with the study of isotope effects on the properties of solids, it must be said that they are, as a rule, expensive and laborious, and also difficult to set up because of the need for relatively large amounts of stable isotopes. In the past, the facilities for separation of isotopes used to work almost exclusively for the military applications, which limited the availability of isotopes for scientific purposes. After the end of the cold war, however, the situation changed, and new stable isotopes have become available. Russian and Western scientists were able to join their efforts in the studies of isotope effects in solids, and this cooperation proved to be very advantageous and successful. Considerable progress has been made in the production of chemically very pure and structurally almost defect-free semiconductor crystals with the predetermined isotopic composition, including highly enriched (almost single-isotope) crystals and materials with highest possible isotopic disorder. For example, large single crystals of diamond, germanium and silicon were fabricated. Extensive studies of isotope effects on static, dynamic and kinetic properties allowed development and validation of various experimental and theoretical approaches, while accomplishing important practical tasks. We may say that now a new direction appeared in applied physics — isotopic engineering of materials [97, 101, 102].

Many specialists from various countries have contributed to the study of isotope effects in solids — far too many to be named here. We can only try to name those whose contribution is really outstanding — Professor M Cardona and his group from Max-Planck-Institut für Festkörperforschung in Stuttgart (lattice constant, phonon and electron spectra of semiconductors, thermal conductivity), Professor E E Haller and K Ito (Lawrence Berkeley National Laboratory, USA — growing of germanium crystals with different isotopic

compositions and study of their properties), T Anthony and W Banholzer (General Electric Company — growing of isotopically modified diamonds and study of their properties), Professor V I Ozhogin (Kurchatov Institute, Moscow — isotopes for semiconductor materials and study of isotope effects).

We thank L A Maksimov for carefully reading the manuscript and giving us his valuable comments and advice. We are also grateful to Yu M Kagan, N A Chernoplekov, and V Yu Baranov for support and concern. The work was partly financed by RFFI (grants Nos 01-02-16508 and 01-02-17469) and CRDF (grant No. RP2-2274).

6. Appendices

Appendix A. Selection of moments

At low temperatures, the phonon – phonon transitions are essentially inelastic. Since only the phonons with small quasimomenta are excited, the umklapp transitions are possible for the nonequilibrium modes that occur only in a certain part of the Brillouin zone. As a result, the transition probability $P(l, l')$ in the regular crystal must depend both on the absolute values of $\mathbf{q}$ and $\mathbf{q}'$ and on their relative orientation in the space of a reciprocal lattice. The normal processes ensure the availability of a finite number of nonequilibrium modes in the region of their most efficient umklapp scattering. The presence of different isotopes in the lattice, from which the phonons experience elastic scattering, gives additional isotropization to the nonequilibrium phonon distribution function $\Phi(l)$. Such an isotropization occurs at temperatures when the rates of inelastic scattering by phonons and elastic scattering by impurities are equal to an order of magnitude. In the case of strong anisotropy of the phonon spectrum (like in germanium), which is associated with the weakly disperse transverse modes, the elastic scattering due to isotopic disorder is also found essentially anisotropic (see, for example, Ref. [45]). Therefore, at low temperatures, because of the U-processes and spectrum anisotropy, it is basically important to explicitly take into account the nonstandard structure of the distribution function $\Phi(l)$. As indicated above, at $T \geqslant T_D/6$ the anharmonic scattering processes of different types are efficient, and all groups of phonons are excited. The role of isotope scattering is then minor. In such a situation, even the standard distribution $\Phi_z(l) \propto v_z\omega(l)$ ought to give an adequate description of the actual distribution with respect to momenta. However, the strong anisotropy of the phonon spectrum can affect the distribution function Φ in this case as well.

In view of this, we would like to present the regular method for construction of linearly independent moments that occur in the expansions for the stationary distribution $\Phi_\alpha(l)$. By definition, $\Phi_\alpha(l) = \omega(l)\tilde{\Phi}_\alpha(l)$ is a periodical piecewise-continuous function with the lattice spacing as a period and exhibiting the point symmetry group of the crystal. Function $\tilde{\Phi}_\alpha(l)$ can be expanded in terms of the functions $g_\alpha^{(i_m)}(l)$, $f_j^{(r_l)}(\mathbf{q})$. Then the moment $g_\alpha^{(i_m)}$ is transformed according to the vector representation and characterizes the angular dependence of the distribution. The moments of the type $f_j^{(r_l)}(\mathbf{q}) = (q/q_D)^a$ $(a = 0, n_r)$ account for the dependence of the distribution on $|\mathbf{q}|$. If $\mathbf{q}$ is given outside the first Brillouin zone, then we must consider the quantity $\mathbf{q} + \mathbf{B}$, where $\mathbf{B}$ is one of the vectors of the reciprocal lattice.

According to the Riesz – Fischer theorem, if $\{\varphi(r)\}$ is the complete orthonormal set of functions, and the sequence of numbers η_r is such that the series $\sum_{r=1}^{\infty}\eta_r^2$ converges, then $\eta_1\varphi^{(1)} + \eta_2\varphi^{(2)} + \ldots$ converges on average to Φ. According to the uniqueness theorem, $\{\eta_r\}$ specify uniquely $\Phi(q)$ almost everywhere in the domain of definition. In particular, if $\Phi(\mathbf{q})$ is continuous, then it is continuous everywhere.

Let us consider the moments of the type $g_\alpha^{(i_m)}$ in greater detail. They are assumed to exhibit the same properties as the components $v^\alpha(l) = \partial\omega(l)/\partial q^\alpha$ of the vector of group velocity. For convenience of notation we shall drop the mode polarization index j in this section.

On the strength of these arguments, for the moments describing the angular dependence of $\Phi_\alpha(\mathbf{q})$ it will be convenient to select functions of the form

$$g_\alpha^{(i_m)}(\mathbf{q}) = v_{\alpha_1}^{(i_1)} \ldots v_{\alpha_j}^{(i_j)}, \quad i_1 + i_2 + \ldots + i_j = m\,, \tag{A.1}$$

where i_s are integers. In the case of cubic crystal, at the symmetry transformations $G \in O_h$ the component $v_\alpha(\mathbf{k})$ is transformed as the basis function of the irreducible representation $\nu = F_{1u}$. The moments (A.1) at $n \neq 1$ realize the basis of the reducible representation $F_{n\nu}$ which is the direct product of n representations Γ_ν:

$$\Gamma_{n\nu} = \bigotimes_{i=1}^{n}\Gamma_\nu\,. \tag{A.2}$$

As for the function Φ_α, it is transformed according to the irreducible representation F_{1u}. Therefore, from the set of moments (A.1) which form the bases of representations (A.2), we must select the functions whose symmetry type is F_{1u}.

In the case of metal with cubic symmetry, the required moments can be found with the aid of the projection operators

$$P^{(\nu)} = \frac{f^{(\nu)}}{g}\sum_G \chi_\nu(G)G\,. \tag{A.3}$$

Here, f_ν is the dimension of the irreducible representation ν, and $\chi_\nu(G)$ is the character of the irreducible representation ν for G. We have

$$g_\nu = P^{(\nu)}g_n\,, \tag{A.4}$$

where g_n is the basis function of the reducible representation $\Gamma_{n\nu}$.

Bearing in mind that the components v_x, v_y, and v_z of the group velocity are transformed under the action of G as the coordinates x, y, and z, we use (A.3) and (A.4) for finding the functions g_ν in a straightforward manner.

The total number of linearly independent functions of the form (A.1) for a certain m is $(m+1)(m+2)/2$. The number of linearly independent moments of the type $\{g_\alpha^{(i_m)}\}$ that occur in the expansion for $\Phi_\alpha(\mathbf{q})$ is much less. This latter number is given by the multiplicity of occurrence of the νth representation of m_ν in the reducible representation $\Gamma_{n\nu'}$. If we know the characters $[\chi^n]G$ of the representation $\Gamma_{n\nu'}$, then

$$m_\nu = \frac{1}{g}\sum_C g_C\chi_\nu(C)[\varkappa^n](C)\,, \tag{A.5}$$

where g_C and g are the numbers of elements in class C and in the group, respectively. By definition, the representation $\Gamma_{n\nu'}$

realized by the functions of the form $v_{\alpha_1}^{(i_1)} \dots v_{\alpha_j}^{(i_j)}$ is symmetrical with respect to all indices $\alpha_1 \dots \alpha_j$. The characters for such representations are found from the following formula [95]

$$[\chi^n]G = \sum_{\{p\}} \frac{\chi^{p_1}(G) \dots \chi^{p_n}(G)}{p_1!2p_2! \dots np_n!}. \qquad \text{(A.6)}$$

In (A.6), p_i are positive integers. Symbol $\{\dots\}$ denotes summation over all possible sets of p_i that satisfy the condition

$$p_1 + 2p_2 + \dots + np_n = n\,.$$

Table A.1 gives the characters of tensor representations $\Gamma_{nv} = \bigotimes_{i=1}^{n} \Gamma_{1u}$ for cubic crystals; m specifies the multiplicity of occurrence of Γ_{1u} in Γ_{nv} and in the equivalent bases (set of linearly independent moments) of the irreducible representation Γ_{1u}.

Table A.1. Characters of tensor representations Γ_{nv} and the equivalent bases for the irreducible representation Γ_{1u}. m is the multiplicity of occurrence of Γ_{1u} in Γ_{nv} for the group O_h.

n	Class					m	Bases
	E	$3C_4^2$	$6C_4$	$6C_2$	$8C_3$		
1	3	−3	1	−1	0	1	x
3	10	−2	0	−2	1	2	x^3, $x(y^2+z^2)$
5	21	−3	1	−3	0	4	x^5, $x^3(y^2+z^2)$, $x(y^4+z^4)$, xy^2z^2
7	36	−4	0	−4	0	6	x^7, $x^5(y^2+z^2)$, $x^3(y^4+z^4)$, $x(y^6+z^6)$, $x(y^4z^2+y^2z^4)$, $x^3y^2z^2$
9	55	−5	1	−5	1	9	x^9, $x^7(y^2+z^2)$, $x^5(y^4+z^4)$, $x^3(y^6+z^6)$, $x(y^8+z^8)$, $x(y^2z^6+y^6z^2)$, $x^3(y^2z^4+y^4z^2)$, $x^5y^2z^2$, xy^4z^4

In addition to crystals with a cubic structure, we shall also consider crystals with hexagonal and tetragonal structures, which possess the point symmetry of groups D_{6h} and D_{4h}, respectively. The coordinate z along the symmetry axis of the fourth order for group D_{4h}, and of the sixth order for D_{6h}, realizes the one-dimensional irreducible representation denoted by A_{2u} for both groups, and the coordinates x and y are the bases of the two-dimensional irreducible representations (E_{1u} for D_{6h}, and E_u for D_{4h}). For this reason, the polynomials of the form $x^i y^j z^k$ can be represented as the product of functions from the bases of tensor representations $\Gamma_n = \bigotimes_{i=1}^{n} A_{2u}$ and $\Gamma_m = \bigotimes_{i=1}^{m} (E_{1u}$ or $E_u)$. The representation Γ_n for all n is one-dimensional; z^n for even n is the basis of A_{1g}, and for odd n the basis of A_{2u}. Table A.2 gives the characters of representations Γ_m for D_{6h} and D_{4h}, and the equivalent bases of representations A_{1g} and E_{1u} (or E_u).

Tables in Ref. [96] give explicit formulas for the simplest vector functions $\mathbf{A}(\mathbf{k})$ compatible with the symmetry of crystals and textures, with the results for most of the crystal classes and textures. Using these tables, one can find the first two or three additional angular moments.

Observe that when the distribution is selected in the form

$$\Phi_z(l) = v_z(l)\,\omega(l)\,F_j(\mathbf{q})\,,$$

Table A.2. Characters of tensor representations Γ_n and Γ_m, and the equivalent bases for irreducible representations A_{1g} (n even) and E_u (n odd) for groups D_{4h} and D_{6h}. Class for D_{4h} is marked with asterisk.

n	Class D_{4h}/D_{6h}							Bases	
	$\frac{E^*}{E}$	$\frac{C_2^*}{C_2}$	$2C_4^*$	$2C_3$	$2C_6$	$\frac{2U_2^*}{3U_2}$	$\frac{2U_2^*}{3U_2}$	D_{4h}	D_{6h}
1	2	−2	−1	0	1	0	0	x	x
2	3	3	0	−1	0	1	1	(x^2+y^2)	(x^2+y^2)
3	4	−4	1	0	−1	0	0	xy^2, x^3	$x(x^2+y^2)$
4	5	5	−1	1	−1	1	1	x^2y^2, x^4+y^4	$(x^2+y^2)^2$
5	6	−6	0	0	0	0	0	x^3y^2, xy^4, x^5	$x(x^2+y^2)^2$, $xy^2(y^2-3x^2)$
6	7	7	1	−1	1	1	1	$x^2y^2(x^2+y^2)$, y^6+z^6	$(x^2+y^2)^3$, $x^6-15x^4y^2+$ $+15x^2y^4-y^6$
7	8	−8	−1	0	1	0	0	x^5y^2, x^3y^4, xy^6, x^7	$x(x^2+y^2)^3$, $x^3(x^4+7y^4)$, $xy^2(y^2-3x^2)\times$ $\times(x^2+y^2)$

by and large the description of the angular dependence can be given in terms of harmonics. They are represented as a combination of spherical harmonics and exhibit the appropriate crystal symmetry. Such harmonics for hexagonal, tetragonal and trigonal crystals are defined in Ref. [97].

Sets of moments of symmetrized and linearly independent $\{g_\alpha^{(i)}\}$ can also be used in the problems of electric conductivity. In particular, they have been used for analyzing the low-temperature electric resistance of metal lithium with the one-sheet Fermi surface. It was assumed that the structure of lithium was cubic. The following moments were taken into account in the solution of the kinetic equation for defining the fine angular structure of the nonequilibrium part of the electron distribution function:

$$g_\alpha^{(1)} = g_s(\mathbf{n}) = \sum_\alpha v_\alpha n_\alpha\,,$$
$$g_\alpha^{(2)} = \sum_\alpha v_\alpha^3 n_\alpha\,,$$
$$g_\alpha^{(3)} = \sum_\alpha v_\alpha^5 n_\alpha\,,$$
$$g_\alpha^{(4)} = (v_x^4 + v_y^4 + v_z^4)\,g_s(\mathbf{n})\,,$$
$$g_\alpha^{(5)} = \sum_\alpha v_\alpha^7 n_\alpha\,,$$
$$g_\alpha^{(6)} = (v_x^6 + v_y^6 + v_z^6)\,g_s(\mathbf{n})\,,$$
$$g_\alpha^{(7)} = \sum_\alpha v_\alpha^9 n_\alpha\,,$$
$$g_\alpha^{(8)} = (v_x^8 + v_y^8 + v_z^8)\,g_s(\mathbf{n})\,,$$

where v_α is the electron group velocity, and $\mathbf{n}$ is the unit vector in the direction of an external field [98, 99].

Notice that in the theory of electric conductivity in the general case of multisheet Fermi surfaces, as a rule, the Fermi-surface harmonics are utilized (see, for example, monographs [98, 99]).

Appendix B. Polarization vectors in a monoatomic lattice

Let us consider the basic equation used for defining the eigenfrequencies $\omega(l)$ and the polarization vectors $\mathbf{e}(k \mid l)$ for the vibrational modes $l = \{\mathbf{q}, j\}$ ($\mathbf{q}$ is the quasi-momentum, j is the polarization index) for the monoatomic crystal with an arbitrary isotopic composition (marked with super-

script c). We have

$$\omega_{\rm c}^2(l)\, e_\alpha^{\rm c}(k \mid l) = \sum_{k',\alpha'} \Phi_{\alpha\alpha'}^{\rm c}(kk' \mid \mathbf{q})\, e_{\alpha'}^{\rm c}(k' \mid l)\,. \qquad (A.7)$$

Here, $\Phi_{\alpha\alpha'}^{\rm c}(kk' \mid \mathbf{q})$ is the dynamic matrix of the crystal, α and α' are the Cartesian indices, k is the number of atomic position in the elementary cell. Matrix Φ is given by the expression

$$\Phi_{\alpha\alpha'}^{\rm c}(kk' \mid \mathbf{q}) = \frac{1}{M_{\rm c}}\,\tilde{\Phi}_{\alpha\alpha'}(kk' \mid \mathbf{q}) = \frac{1}{NM_{\rm c}} \sum_{\mathbf{mm}'} \varphi_{\alpha\alpha'}(\mathbf{m}k, \mathbf{m}'k') \exp\left[\mathrm{i}\mathbf{q}(\mathbf{R}_{\mathbf{m}}^{(0)} - \mathbf{R}_{\mathbf{m}'}^{(0)})\right]. \qquad (A.8)$$

In this equation $\varphi_{\alpha\alpha'}(\mathbf{m}k, \mathbf{m}'k')$ is the matrix of the second-order force parameters, $\mathbf{m}$ is the lattice point vector, and N is the number of elementary cells. Observe that the matrix $\tilde{\Phi}$ does not depend on the mean mass $M_{\rm c}$.

As demonstrated in our study [88], in the case of a monoatomic crystal the frequencies of vibrational modes obey the relationship

$$\frac{{\rm d}\ln\omega_{\rm c}^2(l)}{{\rm d}\ln M_{\rm c}} = -1 + O\left(\left(\frac{\Delta M}{M_{\rm c}}\right)^2, \frac{\Delta M}{M_{\rm c}}\,\frac{\langle u^2\rangle}{a^2}\right). \qquad (A.9)$$

Hence it follows that

$$\omega_{\rm c}(l) = w(l) M_{\rm c}^{-1/2}\,. \qquad (A.10)$$

By definition, the value of $w(l)$ does not depend on $M_{\rm c}$.

Now we substitute (A.10) into (A.7). Using also relation (A.8), we get

$$w^2(l)\, e_\alpha^{\rm c}(k \mid l) = \sum_{k',\alpha'} \tilde{\Phi}_{\alpha\alpha'}^{\rm c}(kk' \mid \mathbf{q})\, e_{\alpha'}^{\rm c}(k' \mid l)\,. \qquad (A.11)$$

From this equation it is immediately seen that, unlike the phonon frequencies, *the polarization vectors* $\mathbf{e}(k \mid l)$ *do not depend on the mass for a particular isotopic composition*.

References

1. Berman R, Foster E L, Ziman J M *Proc. R. Soc. London Ser. A* **237** 344 (1956)
2. Slack G A *Phys. Rev.* **105** 829 (1957)
3. Geballe T H, Hull G W *Phys. Rev.* **110** 773 (1958)
4. Carruthers P *Rev. Mod. Phys.* **33** 92 (1961)
5. Berman R *J. Phys. Chem. Solids* **59** 1229 (1998)
6. Callaway J *Phys. Rev.* **113** 1046 (1959)
7. Bättger H *Principles of the Theory of Lattice Dynamics* (Weinheim: Physik-Verlag, 1983)
8. *Voprosy Kvantovoĭ Teorii Neobratimykh Protsessov* Sbornik stateĭ (Topics in the Quantum Theory of Irreversible Processes: Collection of papers) (Ed. V L Bonch-Bruevich) (Moscow: IL, 1961)
9. Ziman J M *Electrons and Phonons. The Theory of Transport Phenomena in Solids* (Oxford: Clarendon Press, 1960) [Translated into Russian (Moscow: IL, 1962)]
10. Omini M, Sparavigna A *Physica B* **212** 101 (1995)
11. Omini M, Sparavigna A *Phys. Rev. B* **53** 9064 (1996)
12. Omini M, Sparavigna A *Nuovo Cimento D* **19** 1537 (1997)
13. Ladd A J C, Moran B, Hoover W G *Phys. Rev. B* **34** 5058 (1986)
14. Oligschleger C, Schön J C *Phys. Rev. B* **59** 4125 (1999)
15. Jund P, Jullien R *Phys. Rev. B* **59** 13707 (1999)
16. Volz S G, Chen G *Phys. Rev. B* **61** 2651 (2000)
17. Berman R *Thermal Conduction in Solids* (Oxford: Clarendon Press, 1976) [Translated into Russian (Moscow: Mir, 1979)]
18. Casimir H B G *Physica* **5** 495 (1938)
19. Srivastava G P, Verma G S *Can. J. Phys.* **51** 223 (1973)
20. Klemens P G *Proc. Phys. Soc. London Ser. A* **68** 1113 (1955)
21. Inyushkin A V, in *Izotopy: Svoĭstva, Poluchenie, Primenenie* (Isotopes: Properties, Preparation, Applications) (Ed. V Yu Baranov) (Moscow: IzdAT, 2000)
22. Srivastava G P *The Physics of Phonons* (Bristol: A. Hilger, 1990)
23. Herring C *Phys. Rev.* **95** 954 (1954)
24. Simons S *Proc. Phys. Soc. London* **82** 401 (1963)
25. Simons S *Proc. Phys. Soc. London* **83** 749 (1964)
26. Gurzhi R N, Maksimov A O *Fiz. Nizk. Temp.* **3** 356 (1977)
27. Kagan V D, Red'ko N A *Fiz. Tverd. Tela* **33** 1205 (1991) [*Sov. Phys. Solid State* **33** 1358 (1991)]
28. Armstrong B H *Phys. Rev. B* **23** 883 (1981)
29. Armstrong B H *Phys. Rev. B* **32** 3381 (1985)
30. Berman R et al. *Proc. R. Soc. London Ser. A* **253** 403 (1959)
31. Callaway J, von Baeyer H C *Phys. Rev.* **120** 1149 (1960)
32. Berman R, Brock J C F *Proc. R. Soc. London Ser. A* **289** 46 (1965)
33. Thacher P D *Phys. Rev.* **156** 975 (1967)
34. Anthony T R et al. *Phys. Rev. B* **42** 1104 (1990)
35. Onn D G et al. *Phys. Rev. Lett.* **68** 2806 (1992)
36. Graebner J E et al. *Nature* **359** 401 (1992)
37. Wei L et al. *Phys. Rev. Lett.* **70** 3764 (1993)
38. Olson J R et al. *Phys. Rev. B* **47** 14850 (1993)
39. Slack G A *J. Phys. Chem. Solids* **34** 321 (1973)
40. Debye P, in *Vorträge uber die Kinetische Theorie der Materie und der Elektrizität* (Mathematische Vorlesungen an der Universität Göttingen, Bd. 6, Eds M Plank et al.) (Leipzig: B.G. Teubner, 1914) p. 19
41. Leibfried G, Schlömann E *Nach. Akad. Wiss. Göttingen, Math. Phys. Kl.* **4** 71 (1954)
42. Nepsha V I et al. *Dokl. Akad. Nauk SSSR* **317** 96 (1991) [*Sov. Phys. Dokl.* **36** 228 (1992)]
43. Berman R *Phys. Rev. B* **45** 5726 (1992)
44. Asen-Palmer M et al. *Phys. Rev. B* **56** 9431 (1997)
45. Tamura S *Phys. Rev. B* **27** 858 (1983)
46. Holland M G *Phys. Rev.* **132** 2461 (1963)
47. Ozhogin V I et al. *Pis'ma Zh. Eksp. Teor. Fiz.* **63** 463 (1996) [*JETP Lett.* **63** 490 (1996)]
48. Ruf T et al. *Solid State Commun.* **115** 243 (2000)
49. Capinski W S et al. *Appl. Phys. Lett.* **71** 2109 (1997)
50. Touloukian Y S et al. *Thermophysical Properties of Matter* Vol. 1 (The TPRC Data Series, Ed. Y S Touloukian) (New York: IFI/Plenum, 1970)
51. Nilson G, Nelin G *Phys. Rev. B* **6** 3777 (1972)
52. Zhernov A P *Fiz. Tverd. Tela* **41** 1185 (1999) [*Phys. Solid State* **41** 1079 (1999)]
53. Zhernov A P, Zhernov D A *Zh. Eksp. Teor. Fiz.* **114** 1757 (1998) [*JETP* **87** 952 (1998)]
54. Pomeranchuk I *Zh. Eksp. Teor. Fiz.* **12** 245 (1942); see also *Sobranie Nauchnykh Trudov* (Collected Scientific Papers) Vol. 1 (Ed. V B Berestetskiĭ) (Moscow: Nauka, 1972) p. 122
55. Hamilton R A, Parrott J E *Phys. Rev.* **178** 1284 (1969)
56. Capinski W S, Maris H J, Tamura S *Phys. Rev. B* **59** 10105 (1999)
57. Eryigit R, Herman I P *Phys. Rev. B* **53** 7775 (1996)
58. Zhernov A P *Zh. Eksp. Teor. Fiz.* **114** 654 (1998) [*JETP* **87** 357 (1998)]
59. Zhernov A P *Fiz. Nizk. Temp.* **26** 1226 (2000) [*Low. Temp. Phys.* **26** 908 (2000)]
60. Klemens P G *Int. J. Thermophys.* **2** 323 (1981)
61. Maris H J *Phys. Rev. B* **41** 9736 (1990)
62. Tamura S, Shields J A, Wolfe J P *Phys. Rev. B* **44** 3001 (1991)
63. Zyryanov P S, Klinger M I *Kvantovaya Teoriya Yavleniĭ Elektronnogo Perenosa v Kristallicheskikh Poluprovodnikakh* (Quantum Theory of Electron Transport Phenomena in Crystalline Semiconductors) (Moscow: Nauka, 1976)
64. Ansel'm A I *Vvedenie v Teoriyu Poluprovodnikov* (Introduction to Semiconductors Theory) (Moscow: Nauka, 1978) [Translated into English (Moscow: Mir, 1981)]
65. Blatt F J et al. *Thermoelectric Power of Metals* (New York: Plenum Press, 1976) [Translated into Russian (Moscow: Metallurgiya, 1980)]
66. Askerov B M *Elektronnye Yavleniya Perenosa v Poluprovodnikakh* (Electron Transport Phenomena in Semiconductor) (Moscow:

Nauka, 1985) [Translated into English (Singapore: World Scientific, 1994)]
67. Geballe T H, Hull G W *Phys. Rev.* **94** 1134 (1954)
68. Herring C *Phys. Rev.* **96** 1163 (1954)
69. Gurevich É L *Zh. Eksp. Teor. Fiz.* **16** 193 (1946)
70. Tsidilkovskiĭ I M, Kuleyev I G *Semicond. Sci. Technol.* **11** 625 (1996)
71. Kuleev I G et al. *Zh. Eksp. Teor. Fiz.* **114** 191 (1998) [*JETP* **87** 106 (1998)]
72. Oskotskiĭ V S et al. *Fiz. Tverd. Tela* **10** 3247 (1968)
73. Taldenkov A N, Inyushkin A V, Ozhogin V I, Itoh K M, Haller E E, in *Sbornik Dokladov 4-ĭ Vserossiĭskoĭ Nauchnoĭ Konferentsii 'Fiziko-khimicheskie Protsessy pri Selektsii Atomov i Molekul': Zvenigorod, 4–8 Oktyabrya 1999* (Proceedings of the 4th All-Russia Scientific Conference 'Physicochemical Processes under Selection of Atoms and Molecules: Zvenigorod, 4–8 October 1999) (Moscow: TsNIIatominform, 1999) p. 243
74. Taldenkov A N, Inyushkin A V, Ozhogin V I, Itoh K M, Haller E E, in *Trudy 32-go Vserossiĭskogo Soveshchaniya po Fizike Nizkikh Temperatur* (Proceedings of the 32nd All-Russia Conference on the Low-Temperature Physics) (Kazan, 2000)
75. Kozlov V A, Nagaev È L *Pis'ma Zh. Eksp. Teor. Fiz.* **13** 639 (1971) [*JETP Lett.* **13** 454 (1971)]
76. Bel'chik A A, Kozlov V A *Fiz. Tekh. Poluprovodn.* **20** 53 (1986)
77. Zhernov A P, Chulkin E P *Zh. Eksp. Teor. Fiz.* **109** 602 (1996) [*JETP* **82** 321 (1996)]
78. Kagan Yu, Zhernov A P *Zh. Eksp. Teor. Fiz.* **53** 1744 (1967) [*Sov. Phys. JETP* **26** 999 (1968)]
79. Cracknell A P, Wong K C *The Fermi Surface. Its Concept, Determination, and Use in the Physics of Metals* (Oxford: Clarendon Press, 1973) [Translated into Russian (Moscow: Atomizdat, 1978)]
80. Snyder D D, Montgomery D J *Phys. Rev.* **109** 222 (1958)
81. Dugdal J S, Gugan D, Okumura K *Proc. R. Soc. London Ser. A* **263** 407 (1961)
82. Leffler R G, Montgomery D J *Phys. Rev.* **126** 53 (1962)
83. Panova G Kh, Samoĭlov B N *Zh. Eksp. Teor. Fiz.* **53** 1539 (1967) [*Sov. Phys. JETP* **26** 882 (1968)]
84. Babushkina N A, Zhernov A P, Inyushkin A V *Zh. Eksp. Teor. Fiz.* **82** 793 (1982) [*Sov. Phys. JETP* **55** 468 (1982)]
85. Bass J *Adv. Phys.* **21** 431 (1972)
86. Lebedev V I *Teoriya Kubaturnykh Formul i Vychislitel'naya Matematika* (Theory of Cubature Formulas and Computational Mathematics) (Novosibirsk: Nauka, 1980)
87. Zhernov A P *Zh. Eksp. Teor. Fiz.* **114** 2153 (1998) [*JETP* **87** 1172 (1998)]
88. Zhernov A P, Inyushkin A V *Usp. Fiz. Nauk* **171** 827 (2001) [*Phys. Usp.* **44** 785 (2001)]
89. Zhernov A P, Kagan Yu M *Fiz. Tverd. Tela* **20** 3306 (1978)
90. Popovic Z, Carbotte J P, Piercy G R *J. Phys. F: Metal Phys.* **3** 1008 (1973)
91. Pomeranchuk I *Zh. Eksp. Teor. Fiz.* **35** 992 (1959) [*Sov. Phys. JETP* **8** 688 (1959)]
92. Heine V, Cohen L, Weaire D *The Pseudopotential Concept* (Solid State Physics, Vol. 24) (New York: Academic Press, 1970) [Translated into Russian (Moscow: Mir, 1973)]
93. Zernov V B, Sharvin Yu V *Zh. Eksp. Teor. Fiz.* **36** 1038 (1959) [*Sov. Phys. JETP* **9** 733 (1959)]
94. Berman L E et al. *Synchr. Radiat. News* **6** (3) 21 (1993)
95. Kogan V S *Usp. Fiz. Nauk* **78** 579 (1962) [*Sov. Phys. Usp.* **5** 260 (1962)]
96. Cardona M et al. *J. Phys.: Condens. Matter* **5** 61 (1993)
97. Haller E E *J. Appl. Phys.* **77** 2857 (1995)
98. Cardona M *Phys. Status Solidi B* **220** 5 (2000)
99. Plekhanov V G *Usp. Fiz. Nauk* **167** 577 (1997) [*Phys. Usp.* **40** 553 (1997)]
100. Zhernov A P *Fiz. Tverd. Tela* **44** 992 (2002) [*Phys. Solid State* **44** 1035 (2002)]
101. Berezin A A *J. Phys. Chem. Solids* **50** 5 (1989)
102. Plekhanov V G *Usp. Fiz. Nauk* **170** 1245 (2000) [*Phys. Usp.* **43** 1147 (2000)]
103. Petrashen' M I, Trifonov E D *Primenenie Teorii Grupp v Kvantovoĭ Mekhanike* (Applications of Group Theory in Quantum Mechanics) (Moscow: Nauka, 1967) [Translated into English (Cambridge, Mass.: M.I.T. Press, 1969)]
104. Sirotin Yu I, Shaskol'skaya M P *Osnovy Kristallofiziki* (Fundamentals of Crystal Physics) (Moscow: Nauka, 1979) [Translated into English (Moscow: Mir Publ., 1982)]
105. Betts D D, Bhatia A B, Horton G K *Phys. Rev.* **104** 43 (1956)
106. Mertig I, Mrosan E, Ziesche P *Multiple Scattering Theory of Point Defects in Metals: Electronic Properties* (Leipzig: BSB B.G. Teubner Verlagsgesellschaft, 1987)
107. Zhernov A P, Chernoplekov N A, Mrozan É *Metally s Nemagnitnymi Primesnymi Atomami* (Metals with Nonmagnetic Impurity Atoms) (Moscow: Energoatomizdat, 1992)